

DIELECTRIC PERMITTIVITY AND LOSS

Dielectrics can be defined as materials with high electrical resistivities that conduct virtually no electricity at low dc electric fields. A large group of materials, including gases, liquids, semiconductors, ceramics, and organic and inorganic polymers, are classified as dielectrics. There are, however, no perfect dielectric materials.

The study of the electrical properties of dielectrics arises from their practical need for efficient electrical insulation requirements for long operational life. Many dielectric materials are classified by their electrical breakdown strength, dielectric loss, permittivity, and polarization, and these macroscopic properties are related to their atomic and molecular structures. Although dielectrics are widely employed in diverse applications (e.g., capacitors, cables, transformers, and motors), the study of dielectrics has progressed very little since the early investigation of ferroelectric phenomena. However, the advent of microelectronics and complex control devices and components in defence and industrial applications has made dielectric research important in its own right.

The present article reviews briefly the electrostatic concepts that lead to time- and frequency-dependent dielectric phenomena together with the models of dielectric relaxation behavior in various materials. It also includes some explanations for the dielectric aging of insulating materials under high fields in humid environments.

Dielectric Polarization

Static Field. When an electric field is applied to a dielectric material, three processes can occur. A steady flow of direct current (due to the dc conductivity σ_0) may occur if free charges are capable of moving throughout the volume without restraint. Secondly, bound charges can form dipoles by aligning with the field and provide *polarization*. On removal of the field the dipoles may return to their original random orientation with the help of thermal energy, giving rise to *dielectric relaxation*. Thirdly, electronic and ionic charges may hop through the defect sites. These charges are neither free nor bound, and they give rise to an intermediate form of polarization, which involves finite charge storage.

Dielectrics may broadly be divided into nonpolar and polar materials. In nonpolar materials in an external field a dielectric polarization occurs when the positive and negative charges experience an electric force that causes them to move apart in the direction of the external field. As a result, the centers of positive and negative charges no longer coincide. The molecules are then said to be *polarized*, and each molecule forms a dipole and acquires a dipole moment \mathbf{p} , defined thus:

$$\mathbf{p} = e \mathbf{dl} \quad (1)$$

where e is the electronic charge and \mathbf{dl} the displacement ($\sim 10^{-10}$ to 10^{-11} m in magnitude) between the two charge centers. Note that \mathbf{dl} is a vector that points from the negative to the positive charge. Such dipoles are called *induced* dipoles. On removal of the field, the charges are redistributed and the dipole moment vanishes.

2 DIELECTRIC PERMITTIVITY AND LOSS

With polar dielectrics, which lack structural symmetry, the charge centers of opposite polarities do not coincide for a molecule even in the absence of an electric field. However, these molecular dipoles may be randomly distributed, thus summing to a zero dipole moment over any macroscopic volume element (1,2,3,4,5, 6,7,8,9). In the presence of an appropriate electric field, the molecules may align themselves in the field direction and thus provide a net dipole moment.

Macroscopically, the electric field in a dielectric is described (2) by the electric field strength \mathbf{E} (Vcm^{-1}) and the electrical displacement density, also known as the electric flux density, \mathbf{D} ($\text{C}\cdot\text{m}^{-2}$), both \mathbf{D} and \mathbf{E} being vector quantities. Now the polarization can be defined as the dipole moment per unit volume, i.e.,

$$\mathbf{P} = \sum_{i=1}^N \mathbf{p}_i / \Delta v \quad (2)$$

and is also a vector quantity. It should be noted that the normal component of \mathbf{P} at the surface equals the surface charge density per unit area. These three vectors \mathbf{D} , \mathbf{E} , and \mathbf{P} , in a material medium other than vacuum, are related thus:

$$\mathbf{D} = \epsilon_0 \mathbf{E} + \mathbf{P} \quad (3)$$

or

$$\mathbf{D} = \epsilon \mathbf{E} \quad (4)$$

where

$$\epsilon = \epsilon_0 \epsilon_r \quad (5)$$

ϵ_0 is the permittivity in free space ($8.85 \times 10^{-12} \text{ F}\cdot\text{m}^{-1}$), and ϵ_r is the relative permittivity (dimensionless) or the dielectric constant of the material, which takes into account the polarization effect and is defined as

$$\epsilon_r = \frac{C}{C_0} \quad (6)$$

where C_0 is the capacitance of a capacitor with a vacuum between two conductors, and C the capacitance when the same region is filled with the dielectric. ϵ_r is independent of the shape or size of the conductors and is entirely a characteristic of the particular dielectric medium. Table 1 (4) gives the values of ϵ_r for static or low-frequency ($<1 \text{ kHz}$) fields of several materials. ϵ_r , which is a macroscopic and directly measurable parameter, is connected with the microscopic structure of a dielectric material and with its polarization behavior.

From Eq. (3), we have

$$\begin{aligned} \mathbf{D} &= \epsilon_0 \left(1 + \frac{P}{\epsilon_0 E} \right) \mathbf{E} \\ &= \epsilon_0 (1 + \chi) \mathbf{E} \\ &= \epsilon_0 \epsilon_r \mathbf{E} \end{aligned} \quad (7)$$

Table 1: The Relative Permittivity of Some Solid Dielectrics at 25°C (4)

Dielectric	ϵ_r
Vacuum	1 (by definition)
Air (atmospheric pressure, 0°C)	1.0006
Amber	2.7
Borosilicate glass	4.0
Corning glass 0010	6.68
Corning glass 0014	6.78
Pyrex glass	4–5
Quartz (fused)	3.8
Diamond	5.5
Porcelain	5.5
Marble	10–15
Mica	6–11
Steatite	6
Polyethylene	2.25
Polyvinylchloride (PVC)	6
Epoxy resin	3.6–11
Rubber	3–4
Neoprene	7
Beeswax (white)	2.65
Beeswax (yellow)	2.73
Paraffin wax	2.3
Barium Titanate	1200

where

$$\epsilon_r = 1 + \chi \quad \text{and} \quad \chi = \frac{P}{\epsilon_0 E} \quad (8)$$

and χ is the dielectric susceptibility. Thus the parameter χ also provides a link between the macroscopic properties and the atomic–molecular theory of dielectric materials.

We may also write a general relation between P and E thus (8):

$$P = \epsilon \chi E + \text{higher terms in } E \quad (9)$$

where the higher terms in E are applicable to the phenomenon of hyperpolarization. It should be noted that χ is the ratio of bound charge density to free charge density of a capacitor. A measurement of ϵ_r and hence χ provides the magnitude of the polarization P of a dielectric material at any particular field E .

One of the most useful methods of determining P is to measure the current density $J(t)$ as a function of time, as (8)

$$J(t) = \frac{dD}{dt} \quad (10)$$

4 DIELECTRIC PERMITTIVITY AND LOSS

It may be shown (3,8) that for noninteracting dipoles, χ is given by

$$\chi(0) = \frac{NP^2}{3\varepsilon_0 kT} \quad (11)$$

where $\chi(0)$ is the static susceptibility in the zero-frequency limit, N the number density of polarizable molecules, k the Boltzmann constant, and T the temperature. χ is a dimensionless and scalar quantity in an isotropic medium.

Microscopic Concepts of Polarization

We shall consider here the three cases of electronic, ionic, and orientational polarizations.

An isolated neutral atom in an electric field acquires a dipole moment when an external electric field produces a separation of the charge centers of opposite polarities. This is known as the electronic polarization, and it provides an induced dipole moment

$$p_{\text{ind}} = \alpha_e E \quad (12)$$

where α_e is the electronic polarizability of an atom and is given by

$$\alpha_e = 4\pi\varepsilon_0 r_0^3 \quad (13)$$

where r_0 is the radius of the spherical of an electron cloud surrounding an atomic nucleus. The molar polarizability Π of a monoatomic gas is given by

$$\Pi = N_0 \frac{4\pi}{3} r_0^3 \quad (14)$$

where N_0 is the number of molecules in a gram molecule (Avogadro's number). The lowest polarizability belongs to the noble gases with their completely filled outer electronic shells, which screen the nuclei from the effect of the external electric field. For hydrogen, with $r_0 = 0.53 \times 10^{-10}$ m, α_e is 1.66×10^{-41} F·m⁻². Hence for a field E of 10^5 V·m⁻¹, $\alpha E = 10^{-36}$ C·m. The length l of this induced dipole is $p/e = 10^{-17}$ m (e being the electronic charge), which is indeed an extremely small distance compared with atomic dimensions (6).

Ionic polarization occurs in ionic substances, e.g., alkali halides, whose molecules are formed of atoms that have excess charges of opposite polarities. In an external field the relative positions of the positive and negative ions of a molecule may shift, thus introducing the dipole moment in addition to the induced electronic polarization. The ionic polarization p_i is given by

$$p_i = \alpha_i E \quad (15)$$

where α_i is the ionic polarizability of the molecule, which arises from the ionic displacement. The alkali halides (halides of the group I elements) have the highest polarizabilities, possibly because of the single electron in their outermost shells. Table 2 (6) provides a list of values of contribution of ions to the molar polarization of typical alkali halides.

Table 2: Ionic Polarization as a Fraction of the Total Polarization for Alkali Halides, and (in Parentheses) the Ionic Polarization of Each Compound Relative to that of LiF (6)

	F	Cl	Br	I
Li	0.68 (1.0)	0.53 (3.22)	0.49 (1.96)	0.40 (2.09)
Na	0.65 (1.12)	0.50 (3.38)	0.44 (1.82)	0.39 (2.13)
K	0.65 (1.95)	0.49 (4.25)	0.46 (2.38)	0.38 (2.34)
Rb	0.62 (2.19)	0.52 (5.14)	0.44 (2.46)	0.38 (2.62)

The third type of polarization, known as the orientational polarization, is associated with permanent dipoles in dipolar materials that possess a dipole moment even in the absence of an externally applied electric field. However, such a moment may not be observed macroscopically, as the thermal energy will randomize the dipoles so that the average moment will be zero over a small physical volume. On an application of an external electric field the dipoles will experience a torque, which will orient them in the field direction so that the average dipole moment will no longer be zero. It may be shown (3) that the orientational polarizability α_o is given by

$$\alpha_o = \frac{p^2}{3kT} \quad (16)$$

By adding the three polarizabilities mentioned above, the total polarization P can now be written as the sum of the three components, i.e.,

$$P = p_e + p_i + p_o = N \left(\alpha_e + \alpha_i + \frac{p_o^2}{3kT} \right) E \quad (17)$$

where N is the number of contributing molecules or particles per unit volume.

Of course, not all atoms or molecules need display each of these three types of polarizability. Only the orientational polarization is temperature-dependent. Equation (17) is known as the Langevin–Debye formula, and we have

$$\chi = \varepsilon_r - 1 = \frac{P}{\varepsilon_0 E} = \frac{N}{\varepsilon_0} \left(\alpha_e + \alpha_i + \frac{p_o^2}{3kT} \right) \quad (18)$$

Thus a measurement of ε_r as a function of temperature may help to distinguish the orientational polarization contribution from the sum of the components α_e and α_i , which are practically independent of temperature.

Figure 1 shows (9) a plot of $\varepsilon_r - 1$ as a function of $1/T$ for the molecule of methyl amine (CH_5N). The intercept for the line at $1/T = 0$ and its slope are approximately 8×10^{-4} and 0.6 K^{-1} , respectively. From Eqs. (8), (9), and (17), we have (9)

$$\alpha_e + \alpha_i = \frac{8 \times 10^{-4} \varepsilon_0}{N} \approx 6 \times 10^{-4} \text{ F} \cdot \text{m}^2 \quad (19)$$

6 DIELECTRIC PERMITTIVITY AND LOSS

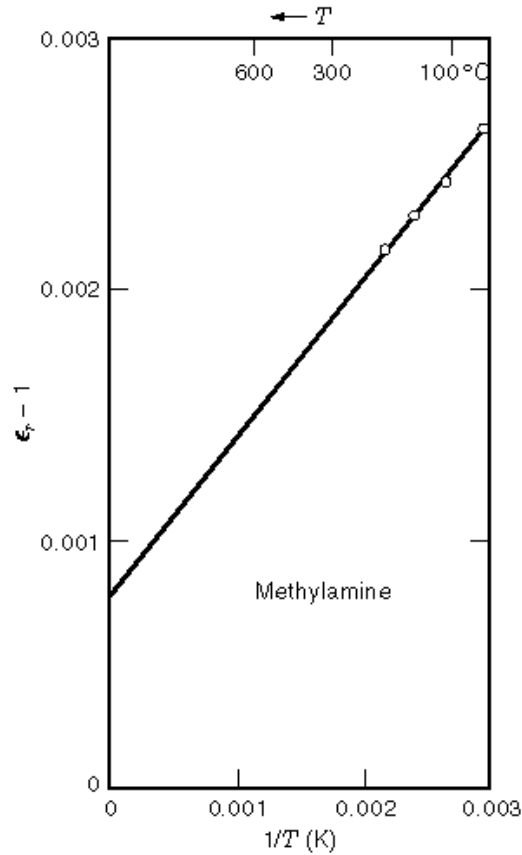


Fig. 1. A plot of $\epsilon_r - 1$ as a function of $1/T$ for a molecule of methylamine (CH_5N) (9,10).

and

$$p_o^2 = \frac{0.6\epsilon_o 3k}{N} \approx 4.2 \times 10^{-30} \text{ C} \cdot \text{m} \quad (20)$$

The further separation of α_e and α_i is not possible using this technique alone.

Table 3 gives the electric dipole moment of some molecules. The commonly used unit of dipole moment is the debye; $1 \text{ D} = 3.33 \times 10^{-30} \text{ C} \cdot \text{M}$.

Space-charge (interfacial) polarization generally arises from a presence of electrons and/or ions that have limited macroscopic motions in the bulk of a dielectric material. Eventually these charge get carriers get localized at lattice defect sites, metal–electrode interfaces, impurity centers, and voids. As a result, the electric field in the dielectric may get distorted, thus producing an apparent increase in the dielectric constant. Space-charge polarization is particularly evident in multiphase and inhomogenous dielectrics, and its effect is dominant, particularly at low frequencies, in practical dielectrics such as impregnated paper, polymers, and sintered ceramics.

Table 3: Electric-Dipole Moments of Some Molecules

Molecule	Dipole Moment	
	(10^{-30} C·m)	(D)
HCl	3.5	1.05
CsCl	35.0	10.5
H ₂ O	6.2	1.87
D ₂ O	6.0	1.80
NH ₃	4.9	1.47
HgCl ₂	0.0	0
CCl ₄	0.0	0
CH ₄ O	5.7	1.71

The study of dielectric polarization and susceptibility in liquids and solids is more complicated than in gases because of the interactions between the atoms and molecules in the condensed phase. These atoms and molecules will still exhibit electronic, ionic, and orientational polarizations. However, the effective local field E_1 on an atom or molecule in a liquid or a solid dielectric may not be the same as the externally applied field E . It is difficult to calculate the effective local field E_1 in the condensed phase except for the most symmetric crystals.

Since $P = \epsilon_0 (\epsilon_r - 1) E$, for the simplest case of a cubic crystal, the Lorentz equation for the local field E_1 (6) is

$$E_1 = (\epsilon_r + 2)E/3 \quad (21)$$

and $P = N\alpha E_1$, where α is the total polarizability and N the number of molecules per unit volume. Hence,

$$P = (\epsilon_r + 2)NE/3 \quad (22)$$

and

$$\frac{N\alpha}{3\epsilon_0} = \frac{\epsilon_r - 1}{\epsilon_r + 2} \quad (23)$$

Equation (23) is the Clausius–Mossotti equation, which relates the microscopic property of the polarizability α with the macroscopic property of the relative permittivity or dielectric constant ϵ_r . Now we have

$$N = \frac{N_0\rho}{M} \quad (24)$$

where N_0 is the Avogadro's number, M the molecular weight, and ρ the density. Substituting Eq. (24) into Eq. (23), we obtain the molar polarizability per mole,

$$\frac{N_0\alpha}{3\epsilon_0} = \frac{M}{\rho} \frac{\epsilon_r - 1}{\epsilon_r + 2} \quad (25)$$

8 DIELECTRIC PERMITTIVITY AND LOSS

Table 4: Polarizability of Argon (9)

Form	T (K)	Pressure (atm)	ϵ_r	α_e ($10^{-40} \text{ F}\cdot\text{m}^2$)
Gas	293	1	1.000517	1.83
Liquid	83	1	1.53	1.86

Table 5: Static and Infinite-Frequency Capacitivity of Some Ionic Crystals (9)

Material	ϵ_r	
	Static	Optical
LiF	9.27	1.90
LiC	11.05	2.68
NaCl	5.62	2.32
KCl	4.64	2.17
RbCl	5.10	2.18
NaI	6.60	2.96

Equation (25) should be used with caution, as it does not take dipolar interactions into account properly. Equation (23) may, however, be used to calculate the electronic polarizability α_e from the measured values of ϵ_r for dilute gases, for which $\epsilon_r \approx 1$ and $\epsilon_r + 2 \approx 3$. For such cases,

$$\alpha_r = \frac{\epsilon_0(\epsilon_r - 1)}{N} = \frac{\epsilon_0\chi}{N} \quad (26)$$

Table 4 shows that the polarizability of the element argon does not vary significantly (9) between its dilute gas and liquid states. That may not be true for other gases with more extensive electronic structure when condensed to liquid or solid form.

The polarizabilities of α_e and α_i may be determined independently for ionic crystals in the solid state. The relative permittivities ϵ_r of ionic crystals are frequency-dependent. For an applied field at low frequencies the value of ϵ_r will be dependent on both α_e and α_i , whereas in the optical frequency range the lattice ions will not be able to follow the applied field and ϵ_r will only be ϵ_e . Table 5 shows the static (low-frequency) and optical (high-frequency) values of ϵ_r for some ionic crystals (9). The difference between the values of ϵ_r in the second and the third column is the contribution of the ionic polarization alone, whereas the third column characterizes the contribution due to α_e .

The behavior of orientational polarization in dipolar molecules in the gas and liquid phases may be quite large if rotation of the dipoles is possible (10). For such a case, the polarizability will have contributions from α_e , α_i , and α_0 , where the α_0 , contribution will be temperature-dependent, ϵ_r increasing with decreasing temperature. However, as the temperature is lowered and the material solidifies, the value of ϵ_r will drop abruptly when the molecules can no longer rotate and thus rotation cannot contribute to the polarization. Figure 2(a) (9,11) illustrates such behaviour of ϵ_r for nitromethane. It may be observed that at 244 K, nitromethane freezes and ϵ_r drops abruptly from 45 to just under 5. At this temperature α_0 is zero for nitromethane and its polarizability arises from the α_e and α_i contributions, which are independent of temperature. However, there are some solids, such as HCl, which do not show this type of behavior. For HCl in the liquid state ϵ_r is large and

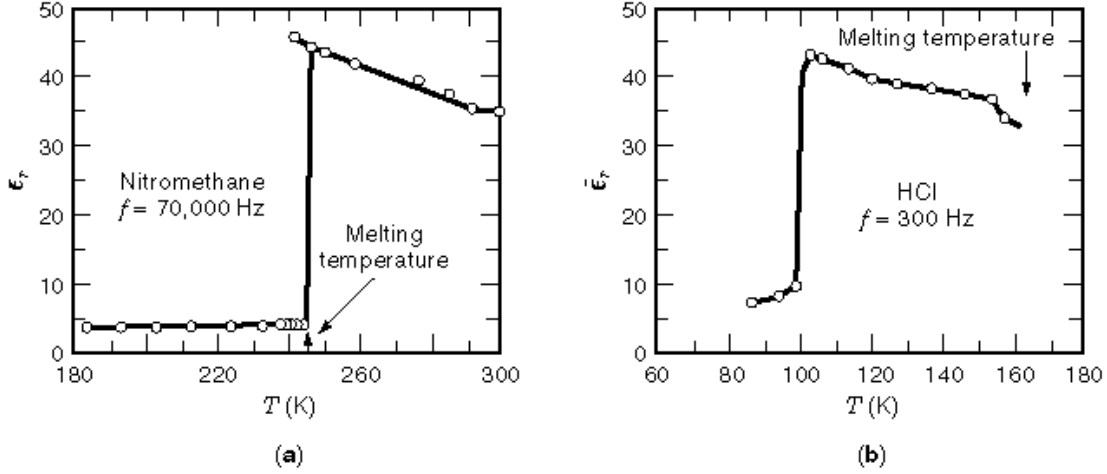


Fig. 2. The behavior of ϵ_r versus T for completely hindered (a) and partly hindered (b) rotation of dipoles in the solid: (a) nitromethane (9,11); (b) hydrogen chloride (9,12).

increases with decreasing temperature, indicating rotational behavior of the molecules [see Fig. 2(b)]. However, below 165 K, where HCl freezes, ϵ_r still continues to increase (9,12) because of the increase in the density of the material. At 100 K, the molecular rotation finally ceases and α_0 virtually becomes zero. The polarization contribution at this temperature in HCl originates from α_e and hindered rotation (9,12).

Dielectric Loss

Time-Dependent Dielectric Response. The dielectric behavior has been represented in the previous section by three vectors \mathbf{D} , \mathbf{E} , and \mathbf{P} , which are assumed to be collinear in space and in the same phase in time. However, neither of these two assumptions is necessarily valid. We shall only consider the nature of the dielectric behavior with time for nonpolar materials and those containing permanent dipoles. As regards the spatial collinearity, extensive treatment of crystal symmetry is necessary and will not be discussed here.

The time-dependent dielectric response may be synthesized (8) from three fundamental time dependences of the electric field, viz., the delta function $\delta(t)$, the step function $1(t)$, and the harmonic function $\sin \omega(t)$ or $\cos \omega(t)$, where ω is the angular frequency ($=2\pi f$). Equation (3) may now be represented thus:

$$\mathbf{D}(t) = \epsilon_0 \mathbf{E} + \mathbf{P}(t)$$

where the first term on the right-hand side provides the instantaneous free-space contribution and the second the delayed polarization. We define a dielectric response function $\phi(t)$. The polarization response to a delta-function excitation of strength $E \Delta t$ is (8)

$$\mathbf{P}(t) = \epsilon_0 (E \Delta t) \phi(t) \quad (27)$$

where E is the electric field, acting over a time period ΔT . From the principle of causality, we have

$$\phi(t) = 0 \quad \text{for } t < 0 \quad (28)$$

10 DIELECTRIC PERMITTIVITY AND LOSS

In the absence of any permanent polarization,

$$\lim_{t \rightarrow \infty} \phi(t) = 0 \quad (29)$$

Furthermore, from the principle of superposition, we have (8)

$$P(t) = \varepsilon_0 \int_{-\infty}^t \phi(t - \tau) E(\tau) dT \quad (30)$$

Equation (29) implies that the magnitude of polarization at a time t in a dielectric will depend on its past value, i.e., the material has a memory. On an application of an elementary step function field $E1(t)$, the dielectric polarization is given by

$$P(t) = \varepsilon_0 E \int_0^t \phi(\tau) d\tau \quad (31)$$

The charging current $I_c(t)$ is given by (8)

$$I_c(t) = \frac{dD(t)}{dt} + \sigma_0 E \quad (32)$$

$$\begin{aligned} &= \varepsilon_0 \frac{dE(t)}{dt} + \frac{dP(t)}{dt} + \sigma_0 E \\ &= \varepsilon_0 E [\delta(t) + \phi(t)] + \sigma_0 E \end{aligned} \quad (33)$$

$$= \varepsilon_0 E [\delta(t) + \phi(t)] + \sigma_0 E \quad (33)$$

where the delta function $\delta(t)$ represents the instantaneous free-space response of the step-function field, followed by the polarization current $dP(t)/dt$ of the material. σ_0 is the dc conductivity, if any, of the dielectric at infinitely long time. Thus, we have (8)

$$P(\infty) = \varepsilon_0 E \int_0^{\infty} \phi(t) dt = \varepsilon_0 \chi(0) E \quad (34)$$

where $P(\infty)$ is the polarization with a steady electric field E after an infinitely long time when the polarizing elements tend to get oriented along the field direction. On removal of this step-function field, a depolarization current $I_d(t)$ will follow as the thermal agitation randomizes the orientation of the dipoles with time. For this latter case there will be no contribution of σ_0 at $E = 0$.

Frequency-Dependent Dielectric Response. The polarization response to a harmonic field is known as the frequency-domain response. Taking the Fourier transform of both sides of Eq. (34), we get

$$P(\omega) = \varepsilon_0 \chi(\omega) E(\omega) \quad (35)$$

where $P(\omega)$ and $E(\omega)$ are the Fourier transforms of the time-dependent polarization and field respectively. $\chi(\omega)$ is the frequency-dependent complex susceptibility, and it is the Fourier transform of the time-dependent response function $\phi(t)$:

$$\chi(\omega) = \chi'(\omega) - i\chi''(\omega) = \int_0^{\infty} \phi(t)e^{i\omega t} dt \quad (36)$$

The real part $\chi'(\omega)$ provides the magnitude of polarization in phase with the harmonic driving field $E(\omega)$ and does not contribute to the power loss, whereas the imaginary part $\chi''(\omega)$, which is in quadrature with the field, is referred to as the dielectric loss. $\chi'(\omega)$ and $\chi''(\omega)$ may be represented as odd and even functions of frequency respectively:

$$\chi'(\omega) = \int_0^{\infty} \phi(t) \cos \omega t dt \quad (37)$$

and

$$\chi''(\omega) = \int_0^{\infty} \phi(t) \sin \omega t dt \quad (38)$$

In terms of permittivity, we may write

$$D(\omega) = \varepsilon(\omega)\mathbf{E}(\omega) = \varepsilon_0[1 + \chi'(\omega) - i\chi''(\omega)]\mathbf{E}(\omega) \quad (39)$$

For zero frequency, i.e., the static case,

$$\chi'(0) = \int_0^{\infty} \phi(t) dt \quad (40)$$

and

$$\chi''(0) = 0 \quad (41)$$

Equation (36) shows that both $\chi'(\omega)$ and $\chi''(\omega)$ are functions of the dielectric response function $\phi(t)$, and these two parameters are Hilbert transforms of each other, through what are referred to as the Kramers–Kronig relations:

$$\chi'(\omega) = \frac{1}{P}C \int_{-\infty}^{\infty} \frac{\chi''(x)}{x - \omega} dx \quad (42)$$

$$\chi''(\omega) = -\frac{1}{P}C \int_{-\infty}^{\infty} \frac{\chi'(x)}{x - \omega} dx \quad (43)$$

12 DIELECTRIC PERMITTIVITY AND LOSS

where C denotes the Cauchy principal value of the integral. For the static case,

$$\chi'(0) = \frac{2}{\pi} \int_{-\infty}^{\infty} \chi''(x) d \ln x \quad (44)$$

Equation (44) indicates that the variation of the dielectric parameters with frequency, i.e., the dielectric dispersion, is an essential property of dielectric materials (8). It also shows that any mechanism that can lead to a strong polarization in a dielectric material must also lead to large losses in some frequency range. In other words, it is not possible to have a loss-free dielectric with a finite susceptibility (8). In most dielectrics the loss is significant only in limited frequency ranges. Figure 3 (8) shows schematically two nonoverlapping loss processes at the low frequencies and a resonance process in the optical frequency range. In a limited frequency region we may define a *high-frequency permittivity* $\varepsilon_{\infty\alpha}$, accounting for all the processes occurring at higher frequencies; thus [see Eq. (39)]

$$\varepsilon(\omega) = \varepsilon_{\infty\alpha} + \varepsilon_0[\chi'_\alpha(\omega) - i\chi''_\alpha(\omega)] \quad (45)$$

from which we get

$$\varepsilon'_\alpha(\omega) = \varepsilon_{\infty\alpha} + \varepsilon_0\chi'_\alpha(\omega) \quad (46)$$

and

$$\varepsilon''_\alpha(\omega) = \varepsilon_0\chi''_\alpha(\omega) \quad (47)$$

For an alternating voltage the frequency-dependent complex capacitance $C(\omega)$ is

$$C(\omega) = C'(\omega) - iC''(\omega) \quad (48)$$

where $C'(\omega)$ and $C''(\omega)$ are the real and imaginary parts of the complex capacitance. The loss angle δ is the angle between the electric field and the dielectric polarization. The loss tangent,

$$\tan \delta = \frac{C''(\omega)}{C'(\omega)} = \frac{\varepsilon''(\omega)}{\varepsilon'(\omega)} \quad (49)$$

is independent of the geometry of the dielectric material.

The existence of the polarization with respect to the field leads to the energy dissipation in the dielectric. Now the power dissipation per unit volume is

$$\underline{P} = I_{\text{phase}}E$$

where I_{phase} is the part of the current in phase with E , and is given by

$$\underline{P} = \omega E^2 \varepsilon_0 \varepsilon' \tan \delta = \omega E^2 \varepsilon_0 \varepsilon'' \quad (50)$$

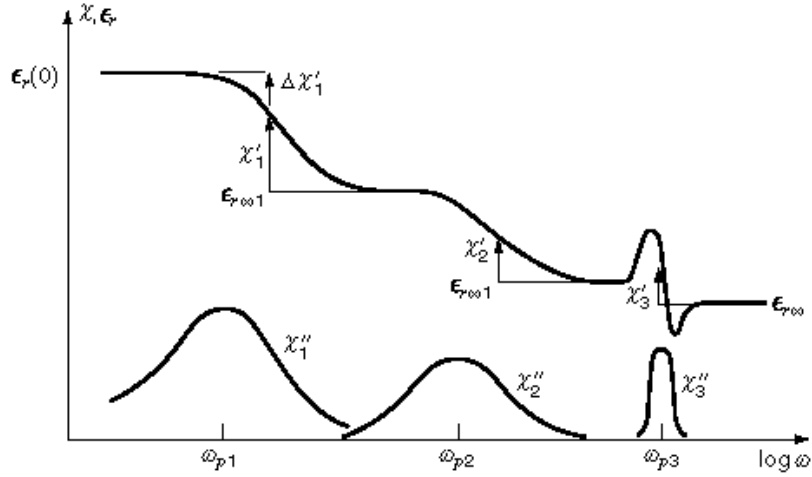


Fig. 3. Schematic diagram of the frequency dependence of the real and imaginary parts of the complex susceptibility, showing three processes, the last one being a resonance process (8).

Table 6 gives (6) typical values of the permittivity and loss factor of various dielectric materials at room temperature for different frequencies. Generally polar materials have larger permittivities and loss tangents than nonpolar materials. For many liquids the frequency at which maximum energy loss occurs at room temperature is approximately 1000 MHz (wavelength $\lambda \approx 0.3$ m), as shown (1) for three typical liquids in Table 7, where τ is the relaxation time ($=1/f$).

Another type of energy loss occurs in a resonance absorption process at very high (i.e., IR, visible, and UV) frequencies. Although the real and imaginary parts of the complex permittivity vary in a similar manner to that for dipole relaxation, the origin of the energy loss is different in this process. At optical frequencies the permittivity of the dielectric is almost entirely due to the electronic polarization. In the absence of any external field a vibrating electron of charge e and mass m is elastically bound to its nucleus by a restoring force, and its equation of motion is

$$m \frac{d^2x}{dt^2} + kx = 0 \quad (51)$$

where k is the restoring-force constant and x is the displacement of the electron. The above equation represents a simple harmonic motion, and its solution is

$$x = x_0 \sin \omega_0 t + A \quad (52)$$

where $\omega_0 = (k/m)^{1/2}$, A is the integration constant, x_0 the amplitude of oscillation, and ω_0 the natural resonance angular frequency of the oscillation. When an external alternating electric field is applied to this system, the resulting motion is a forced oscillation, represented by

$$m \frac{d^2x}{dt^2} + m\omega_0^2 x = eE \cos \omega t \quad (53)$$

14 DIELECTRIC PERMITTIVITY AND LOSS

where E is the amplitude of the field \mathbf{E} and ω is its frequency. Clearly the response of the oscillating system will now depend on both ω and ω_0 . The oscillations might be expected to build up without limit when $\omega = \omega_0$, though they are expected to be small at frequencies far away from ω_0 . However, at resonance, i.e., $\omega = \omega_0$, the oscillations will in fact be limited (damped) by the emission of electromagnetic radiation by the oscillating charges, which dissipates energy. It may be shown that in a resonance absorption process (6),

$$\varepsilon'(\omega) = \varepsilon_0 + \frac{Ne^2}{m} \frac{\omega_0^2 - \omega^2}{(\omega_0^2 - \omega^2) + r^2\omega^2} \quad (54)$$

and

$$\varepsilon''(\omega) = \frac{Ne^2}{m} \frac{r\omega}{(\omega_0^2 - \omega^2) + r^2\omega^2} \quad (55)$$

where r is a constant of the material, called the dissipation constant. These quantities have the form shown in Fig. 3 at very high frequencies. For $\omega = 0$, i.e., the static case, we have

$$\varepsilon'(0) = \varepsilon_0 + \frac{Ne^2}{m\omega_0^2} \quad (56)$$

$\varepsilon''(\omega)$ approaches zero for both $\omega \gg \omega_0$ and $\omega \ll \omega_0$, and it goes through a maximum value of $Ne^2/(mr\omega)$. Again $\varepsilon''(\omega)$ represents an energy loss and the power loss is given again by

$$\underline{P} = \omega\varepsilon''(\omega)\varepsilon_0\mathbf{E}^2 \quad (57)$$

As the characteristic values of ω_0 for electron clouds are very high, the resonance absorptions and their corresponding energy losses occur at very high frequencies, i.e., in the IR-to-UV range.

For pure nonpolar dielectrics, whether solid, liquid, or gas, the polarization is essentially of electronic nature. Some polar materials with a highly symmetric structure, like carbon tetrachloride (CCl_4), may also exhibit electronic polarization. The presence of electronic polarizability may be verified with the Maxwell relation, $\varepsilon^1 = n^2$, where n is the refractive index of the dielectric. Table 8 compares the ε^1 and n^2 values for a few marginally nonpolar materials (13,14).

Models of Dielectric Relaxation

Models. The first model of the dielectric relation is due to Debye (3). According to this model, the susceptibility function $\chi(\omega)$ for noninteracting polar molecules is given by (7)

$$\chi(\omega) \propto \frac{1}{1 + i\frac{\omega}{\omega_p}} \quad (58)$$

Table 6: Dielectric Properties of Materials (6)

Material	Direction	Relative permittivity ϵ_r				Loss tangent $\tan \delta$
		$f = 60$ Hz	100 kHz	1 MHz	100 MHz	
<i>Crystals</i>						
Rutile, TiO ₂	$\parallel c$	—	170	170	—	10^{-4}
	$\perp c$	—	90	90	—	2×10^{-4}
Aluminium oxide, Al ₂ O ₃	$\parallel c$	—	10.6	10.6	10.6	—
	$\perp c$	—	8.6	8.6	8.6	—
Lithium niobate, LiNbO ₃	$\parallel c$	—	—	30	—	0.05
	$\perp c$	—	—	75	—	—
<i>Ceramics</i>						
BaTiO ₃	—	—	—	1600	—	150×10^{-4}
Alumina	—	—	—	4.5–8.5	—	0.0002–0.01
Steatite	—	—	—	5.5–7.5	—	0.0002–0.004
Rutile	—	—	—	14–110	—	0.0002–0.005
Porcelain	—	—	—	6–8	—	0.003–0.02
<i>Polymers</i>						
Polyethylene	—	—	2.3	2.3	—	10^{-4} – 10^{-3}
Polypropylene	—	2.1	—	—	—	2.5×10^{-4}
PTFE	—	2.1	2–3	2–3	—	2×10^{-4}
Polystyrene	—	2.55	—	—	—	5×10^{-5}
PVC	—	3–6	3–5	3.5	3.0	10^{-4}
Polycarbonate	—	—	—	2.8	—	3×10^{-2}
Polyester	—	—	—	4–5	—	0.02
Nylon 66	—	—	3.5	3.33	3.16	0.02
<i>Glasses</i>						
Pyrex	—	—	—	—	4–6	0.008–0.025
Quartz	—	—	—	4	—	2×10^{-4}
Vycor	—	—	—	—	3.8	9×10^{-4}
<i>Miscellaneous</i>						
Mica	—	—	—	5	—	3×10^{-4}
Neoprene	—	—	—	6.3	—	—

where ω_p is the angular frequency at which the maximum loss peak occurs. The real and imaginary parts of $\chi(\omega)$ are

$$\chi''(\omega) \propto \frac{1}{1 + \omega^2 \tau^2} \quad (59)$$

Table 7: Typical Relaxation Times of Three Liquids (9)

Material	Temperature (°C)	τ (10^{-11} s)
H ₂ O	19	1
CH ₃ OH	19	6
C ₂ H ₅ OH	20	13

Table 8: A Comparison of ϵ' and n^2 Values for Several Nonpolar Materials (13, 14)

Material	n^2	ϵ'	Frequency of measurement of ϵ' (Hz)
Hydrogen (liquid, -253°C)	1.232	1.228	
Diamond	5.66	5.68	
Nitrogen (liquid, -197°C)	1.453	1.454	
Oxygen (liquid, -190°C)	1.491	1.507	
Chlorine (liquid)	1.918	1.910	
Bromine	2.66	3.09	
Paraffin (liquid)	2.19	2.20	10^3
Benzene	2.25	2.284	10^3
Polystyrene	2.53	2.55	10^2 to 10^{10}
Polyethylene	2.28	2.30	10^2 to 10^{10}
Carbon tetrachloride	2.13	2.238	
PTFE	1.89	2.10	10^2 to 10^9

and

$$\chi''(\omega) \propto \frac{\omega\tau}{1 + \omega^2\tau^2} \quad (60)$$

The corresponding time-domain response $\phi(t)$ follows the exponential function (15)

$$\phi t \propto e^{-t/\tau} \quad (61)$$

The loss peak occurs here at $\omega = \omega_P = 1/\tau$. Figure 4 shows the dependence of $\chi'(\omega)$, $\chi''(\omega)$, and $\phi(t)$ of Eqs. (59, 60, 61) (16) in log-log representation. The loss peak is symmetric about ω_P , and its width at half height is 1.144 decades on the frequency scale. The Debye behavior has been observed in gases and in some polar liquids. The relaxation behavior of water and deuterium oxide closely approximates that of the Debye form (17,18,19). However, it is generally nonexistent in solids.

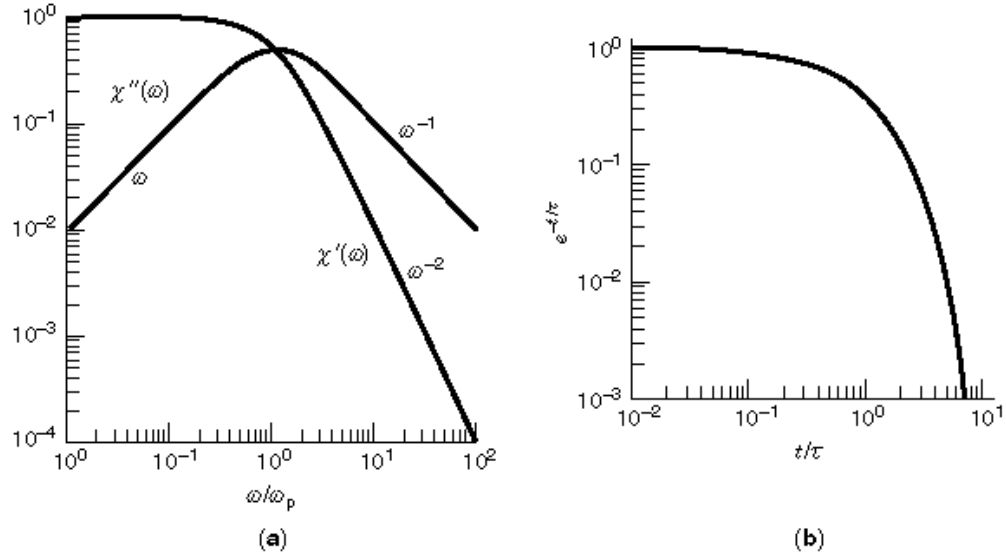


Fig. 4. (a) The ideal Debye response in the frequency domain, with its characteristic frequency dependence of $\chi'(\omega) \propto \omega^{-2}$ and $\chi''(\omega) \propto \omega^{-1}$ above the loss peak. (b) The corresponding time-domain response, which is purely exponential and is here plotted in the somewhat unfamiliar log–log representation (16).

To account for the departure of the observed dielectric behavior, the following empirical expressions have been proposed. The Cole–Cole equation (20) is

$$\chi(\omega) \propto \frac{1}{1 + (i\omega/\omega_p)^{1-\alpha}} \quad (62)$$

where α is a fitting parameter in the range $0 < \alpha \leq 1$. Equation (60) provides a broader, and symmetrical relaxation spectrum than the Debye type. Furthermore, for $\omega > \omega_0$, $\chi'(\omega)$ and $\chi''(\omega)$ show parallelism in the log–log plot.

The Davidson–Cole equation has the form (21)

$$\chi(\omega) \propto \frac{1}{(1 + i\omega/\omega_p)^\beta} \quad (63)$$

where β is yet another curve-fitting parameter in the range $0 < \beta \leq 1$. Equation (61) provides asymmetric relaxation profiles at $\omega \leq \omega_0$, whereas $\chi'(\omega)$ and $\chi''(\omega)$ remain parallel at $\omega > \omega_0$.

The Fuoss–Kirkwood model (22) for the imaginary part of the susceptibility is

$$\chi''(\omega) \propto \frac{2(\omega/\omega_p)^\gamma}{1 + (\omega/\omega_p)^{2\gamma}} \quad (64)$$

18 DIELECTRIC PERMITTIVITY AND LOSS

Another relaxation model is given by

$$\chi(\omega) \propto \sum_{s=1}^{\infty} \frac{\Gamma(\Delta s)}{(s-1)!} \left(\frac{\exp(-i\Delta\pi/2)}{\omega^\Delta \omega_p^{-\Delta}} \right)^s \quad (65)$$

This is an expansion into the frequency domain of the Kolrauch–Williams–Watts function (15) of time, i.e., $\exp[-(t/\tau)^\Delta]$. The parameter Δ in Eq. (65) has no physical significance and is not based on the physics of dielectric interactions.

So far the models have had only one fitting parameter, viz., α for the Cole–Cole equation, β for the Davidson–Cole equation, γ for the Fuoss–Kirkwood equation, and Δ for the Kolrauch–Williams–Watt equation. The model due to Havriliak and Negami (23,24), the first one with two parameters, is given by

$$\chi(\omega) \propto \frac{1}{\left[1 + (i\omega/\omega_p)^{1-\alpha} \right]^\beta} \quad (66)$$

It should be stressed again that the fitting parameters α and β in the above equation have no physical significance.

A classical form of presentation of the dielectric data is to plot $\chi'(\omega)$ or $\varepsilon'(\omega)$ against $\chi''(\omega)$ or $\varepsilon''(\omega)$, i.e., the so-called Cole–Cole plot (20). Figure 5 shows the shapes of the Debye, Cole–Cole, and Davidson–Cole equations for the susceptibility functions in Cole–Cole plots. It has been shown (20) that with the Debye model, a graph of $\chi'(\omega)$ against $\chi''(\omega)$ over the entire frequency range will be a semicircle and $\chi(\infty)$ or ε_∞ is obtained from the intercept at the horizontal axis [see Fig. 5(a)]. Thus the relaxation time τ may be obtained from the slope of a straight line from the origin to a point on the semicircle for which ω is known. Now the Cole–Cole relaxation model provides a symmetrical but broader relaxation spectrum, and the corresponding Cole–Cole plot is still a semicircle. However, its center is depressed below the χ' or ε' horizontal axis [see Fig. 5(b)] with the angle $\alpha\pi/2$ between the radius of the circle and χ' or ε' axis. There is no molecular interpretation of this factor α , and it has been interpreted as a “spreading factor” of the actual relaxation time about a certain mean value. The magnitude of α must lie between zero and unity. The Cole–Cole plot for the Davidson–Cole model is a skewed plot [see Fig. 5(c)], representing a severe departure from the Debye relaxation behavior.

The Havriliak–Negami function (23,24) with two parameters α and β [Eq. (66)] appears to provide the best results for the fitting of the measured dielectric data for most materials. However, none of these mathematical models that invoke a distribution of relaxation energies (25) or times offer any physical interpretation of material properties (26,27,28,29).

It has been suggested that a dielectric loss spectrum may be regarded as a mathematical summation of a distribution function $g(\tau)$ of Debye responses corresponding to a distribution of relaxation times (30); thus

$$\chi(\omega) = \int_0^{\infty} \frac{g(\tau)}{1 + i\omega\tau} d\tau \quad (67)$$

The distribution functions are always positive, and curves of $\chi''(\omega)$ or $\varepsilon''(\omega)$ can be formed from them by the superposition of many single relaxation-time or frequency curves (31). It has been shown (32) that the product of the elapsed time and the depolarization current is a convolution of the distribution function of relaxation frequencies with a weight function of an asymmetric bell shape. A similar relationship is also shown to exist for the imaginary part of the permittivity. The same work (32) also proposes a deconvolution procedure to determine

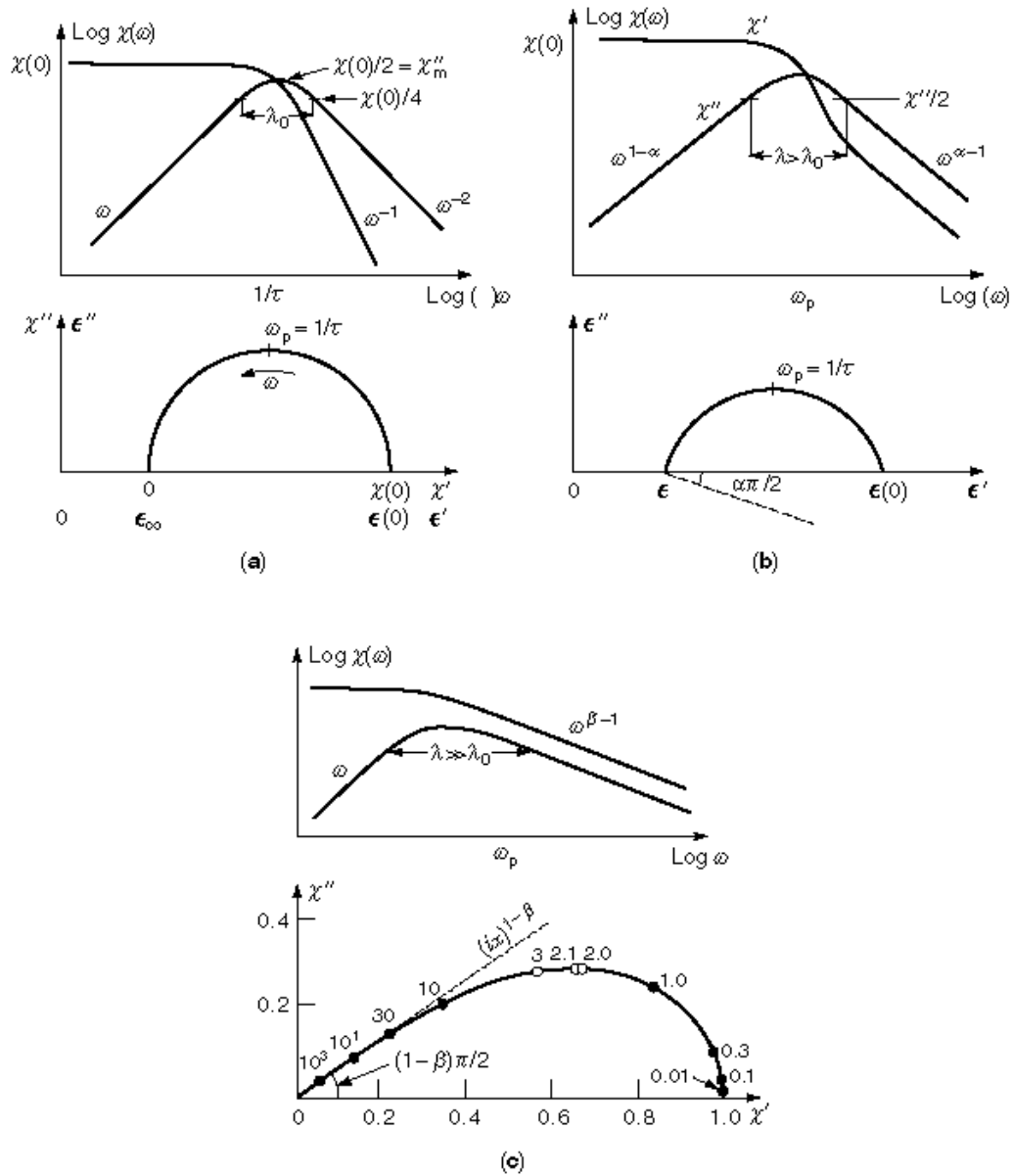


Fig. 5. The frequency dependence of the real and imaginary parts of the susceptibility and the Cole–Cole presentation for (a) Debye, (b) Cole–Cole, (c) Davidson–Cole systems (8).

the distribution function of relaxation frequencies from experimental data. A distribution of relaxation times from the frequency dependence of the real part of the complex permittivity has also been made with the inverse Fourier transformation (33). As stated earlier, however, no distribution of relaxation times that can claim physical reality can be associated, with relaxation systems in condensed matter (8,26,27).

20 DIELECTRIC PERMITTIVITY AND LOSS

A two-parameter model for the complex susceptibility function $\chi(\omega)$, known as the *universal relaxation law*, has been proposed (8,16), which states that all solid dielectrics follow fractional power laws in frequency. It is of interest to note that $\chi(\omega)$ may be expressed by a simple empirical expression (16,23),

$$\chi(\omega) = A[1 + (ix)^m]^{(n-1)/m} \quad (68)$$

where the exponents m and n lie between zero and unity, and x is the normalized frequency. Equation (68) indicates that the experimental state of dielectric susceptibility can be fitted with two power-law exponents. The Debye function is a limiting form of the above equation for $m = 1$ and $n = 0$. For the symmetric loss peak at ω_p and $x = 1$, we have $m = 1 - n$. Furthermore, the ratio $\chi''(\omega)/\chi'(\omega)$ decreases as m and $1 - n$ become smaller, thus providing broader peaks as in the case of the Cole–Cole function. This leads to the universal law, characterized by two fractional power laws in frequency respectively below and above the loss-peak frequency ω_p (8,16),

$$\chi''(\omega) = \tan\left(\frac{m\pi}{2}\right) [\chi(0) - \chi'(\omega)] \propto \omega^m \quad \text{for } \omega \ll \omega_p, \quad (69)$$

for $\omega \ll \omega_p$, and

$$\chi''(\omega) = \cot\left(\frac{n\pi}{2}\right) \chi'(\omega) \propto \omega^{n-1} \quad \text{for } \omega \gg \omega_p \quad (70)$$

where the exponents are in the range

$$0 < n < 1 \quad \text{and} \quad 0 < m < 1$$

As a result, in the high-frequency range of the loss peak, the ratio of the imaginary to the real part of the complex susceptibility is a frequency-independent constant,

$$\frac{\chi''(\omega)}{\chi'(\omega)} = \cot\left(\frac{n\pi}{2}\right) \quad (71)$$

Hence, in a log–log plot $\chi''(\omega)$ and $\chi'(\omega)$ appear as parallel lines for $\omega \gg \omega_p$. It should be noted that for the Debye process this ratio is $\omega\tau$ and thus increases linearly with frequency, which is consistent with the idea that the process is a “viscous” phenomenon in which the dielectric loss is linearly related to the angular velocity (16).

For the low-frequency part of the loss peak ($\omega < \omega_p$), we have (8,15)

$$\frac{\chi''(\omega)}{\Delta\chi'(\omega)} = \tan\left(\frac{m\pi}{2}\right) \quad (72)$$

where $\Delta\chi'(\omega) = \chi(0) - \chi'(\omega)$ is known as the *dielectric decrement* and is the extent to which the polarization at any particular frequency falls short of the value of the equilibrium polarization in a static field. The equations (69) and (70) may be represented by the empirical law combining the two fractional power laws above and

below ω_p (8),

$$\chi''(\omega) \propto \frac{1}{(\omega/\omega_p)^{-m} + (\omega/\omega_p)^{1-n}} \quad (73)$$

The Fourier transforms of fractional power laws correlate the frequency-domain dielectric parameters with their time-domain behavior thus (16):

$$\omega^m \propto t^{-m-1} \quad \text{for } t \gg \tau \quad (74)$$

$$\omega^{n-1} \propto t^{-n} \quad \text{for } t \ll \tau \quad (75)$$

In the carrier-dominated low-frequency dispersion (*LFD*) or quasi-dc (*QDC*) systems, mobile charge carriers, such as ions and electrons, act as polarizing species and provide a broad dielectric response (16,34,35,36) in which no loss peak is observed. The *LFD* (or *QDC*) relaxation is characterized by two independent processes, below and above a certain critical frequency ω_c , which may be represented by Eq. (70). The real and imaginary parts of the complex dielectric susceptibility steadily increase with decreasing frequency for small values of n_2 , at frequencies less than ω_c . This is followed by a flat loss behavior above ω_c with $n_1 \approx 1$ (8,16,28). The frequency ω_c plays an analogous role to ω_p in a dipolar system.

Figure 6 shows (16) typical behavior of $\chi(\omega)$ for the *LFD* (or *QDC*) system. Figure 7 shows schematically the typical time-domain behavior of a dipolar *LFD* (or *QDC*) system together with the flat loss response corresponding to $n \rightarrow 1$ (15). Note that the flat loss behavior is the limiting case of the dielectric response that occurs in low-loss materials with a very small value of the ratio $\chi''(\omega)/\chi'(\omega)$. The value of n_2 can never be zero, and hence n cannot actually have a value of 1, although nearly flat loss behavior has been observed experimentally.

There are few examples of solids, including single crystals of ferroelectrics, that show pure Debye relaxation behavior. A variety of solids—viz., low-loss dielectrics, dipolar materials, semiconductor *p-n* junctions, and biological materials—are known to show dielectric dispersions that may be fitted with the universal fractional power law Eq. (73). Furthermore, dipolar systems exhibit loss peaks, whereas the carrier-dominated systems exhibit *LFD* (or *QDC*) behavior (8,34,35).

A stochastic model for the universal dielectric dispersion has also been proposed in recent years (37,38,39). This probabilistic model is based on the assumption that individual dipoles and their environment interact during the process of relaxation and the dielectric response function is given by (37)

$$\phi(t) = \phi_0 \alpha \omega_p (\omega_p t)^{\alpha-1} [1 + k(\omega_p t)^\alpha] \quad (76)$$

where ϕ_0 is a constant of the relaxation function $\phi(t)$, and k is a positive real number. In the short-time limit this function is

$$\phi(t) \approx (\omega_p t)^{\alpha-1} = (\omega_p t)^{-n} \quad (77)$$

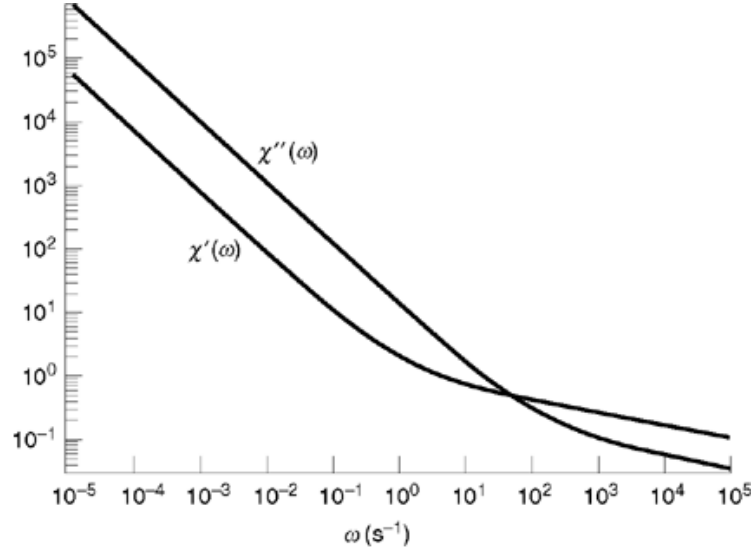


Fig. 6. The frequency dependence of a system dominated by *LFD* or *QDC* with $n_1 = 0.8$ at high frequencies and $n_2 = 0.5$ at low frequencies. The crossover point is deliberately shifted to high frequencies to show the *LFD* or *QDC* region (16).

where $n = 1 - \alpha$ and $0 < n < 1$. The corresponding long-time limit is

$$\phi(t) \approx (\omega_p t)^{-(\alpha+k)/k} = (\omega_p t)^{-m-1} \quad (78)$$

where $m = \alpha/k$ and $0 < m < 1$ if $\alpha < k$. The exponents m and n of the universal fractional law (8) are thus related by (37)

$$m = \frac{1 - n}{k} \quad (79)$$

where $k > 1 - n$ and $0 < n < 1$. If $1 - n < k \leq 1$, then $1 - n \leq m < 1$, and this is observed in most analyzed experimental results. For $k = 1$ we have $m = 1 - n$, and this is the Cole–Cole response. For $k = 1 - n$ we have $m = 1$, which is the Davidson–Cole response. If $k > 1$, then $0 < m < 1$, which is observed only in a small number of analyzed data (21,33,38). In the case, $k \rightarrow 0$ and the Williams–Watts response is observed (15,40). The probabilistic model (37,38,39) thus suggests a relation between the empirical parameters m and n , defining the low- and high-frequency regions of the complex dielectric susceptibility. It has been suggested (37) that the parameter (k) may be related to the waiting-time distribution of the relaxing dipoles, which may follow a Weibull distribution, viz.,

$$R(s) = \exp(-ks^\delta) \quad (80)$$

where $R(s)$ is the waiting-time distribution, k is a positive real number, and $0 < \delta < 1$. It has been shown (37) that for a particular waiting-time distribution function, the solution for $\phi(t)$ can be obtained in a simple analytical

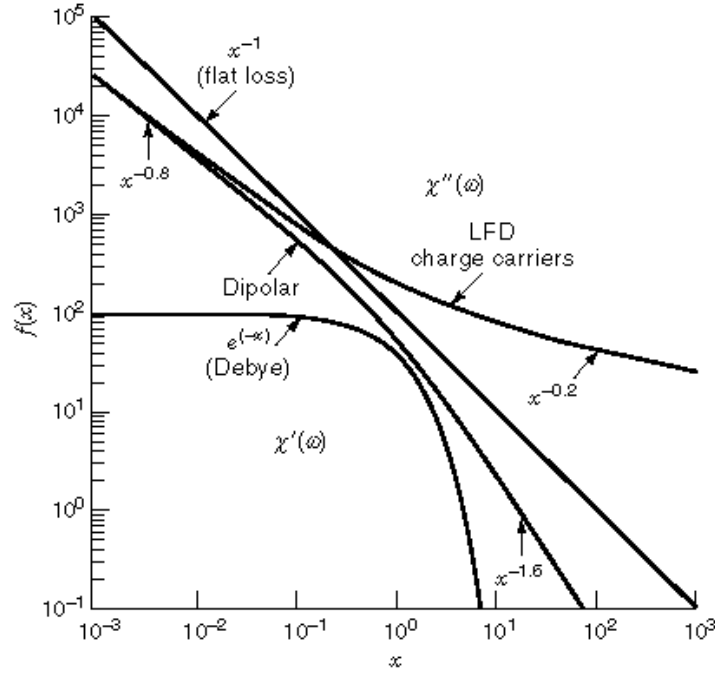


Fig. 7. The time-domain response $\phi(t/\tau)$ of typical dielectric systems, including the Debye exponential response; the dipolar response with $n = 0.8$, $m = 0.6$; the carrier-dominated *LFD* response with $n_1 = 0.8$, $n_2 = 0.2$; and the flat loss with $n = 1$ (16).

form,

$$\phi(t) = \phi(t, 1 - n, k), \quad 0 < 1 - n < 1 \quad \text{and} \quad k > 0 \quad (81)$$

The relatively recent model (41,42) based on a cluster theory is perhaps the most sophisticated approach to the explanation of observed relaxation phenomena in imperfect materials. The theory has been derived in the framework of quantum mechanics and takes into account the many-body interactions present in condensed matter.

The dipoles in the condensed phase may be regarded as connected with other dipoles through their morphological structure, and it is unlikely that they can act independently as in the Debye model. Both solids and liquids are composed of spatially limited regions possessing partially regular structural order, and such regions may be called *clusters* (41). In any material many clusters may exist, and in the presence of coupling between them an array may form displaying partial long-range order. Absence of coupling in the limit may lead to a *cluster gas*. In contrast, systems with strong coupling between these arrays will produce an almost perfect crystal. The model also considers two kinds of interactions, viz., intracluster and intercluster exchanges, and each of these makes its own contributions to the final behavior of the complex susceptibility function.

A dipole in the intracluster motion may first relax exponentially ($d^{-t/\tau}$) as suggested in the Debye model. In doing so, it will affect the field experienced by other neighboring dipoles in the cluster. These neighboring dipoles, in turn, may also relax exponentially, thereby affecting the field experienced by the first dipole, and so on. As a result, the overall effect will be a process with an exponential single dipole relaxation of the form $e^{-t/\tau}$ and concomitant t^{-n} behavior for the relaxation of the cluster dipole moment. The intercluster exchange will have a larger range than for the intracluster motion, and its origin is in dipoles near the edge of the cluster

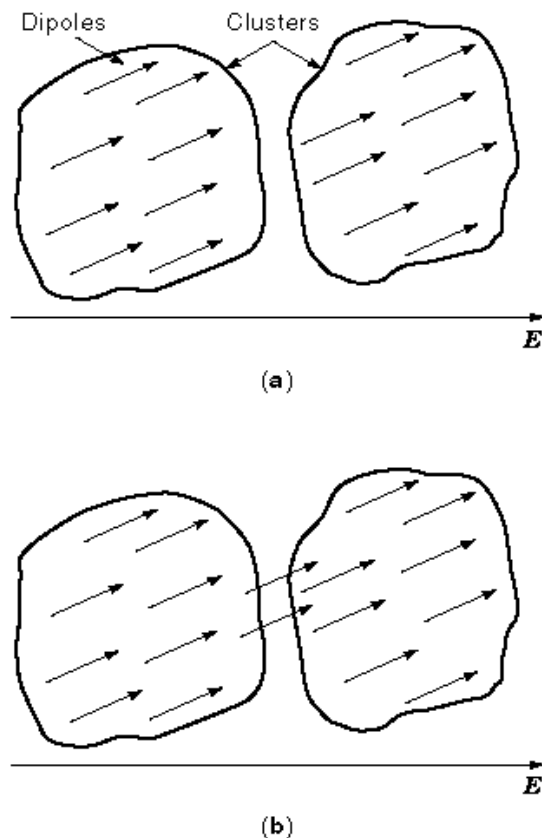


Fig. 8. Schematic diagram of (a) intracuster motion and (b) intercluster exchange mechanism of Dissado–Hill model of dielectric relaxation (29,36).

interconnecting to a neighboring cluster (29,36,40). It has been shown (41) that with the intracuster motion and with the progressive involvement of an increasing number of elements with the progress of time, a fractional power law (i.e., ω^{n-1} behavior) for the susceptibility function may be obtained. Furthermore, the parameter n ($0 < n < 1$) is related to the average cluster structure. Highly ordered structure has n -values approaching unity, thus indicating an existence of completely correlated clusters. On the other hand, $n \rightarrow 0$ would signify a large degree of disorder, and the limit $n = 0$ would yield Debye-like relaxation behavior.

The intracuster coupled mode may change to an intercluster mode as the spatial extent of the coupling (wavelength) increases beyond the cluster size. The mathematical derivation of the susceptibility function for the intercluster exchanges is similar to that of the intracuster motion, the intercluster exchanges now being the perturbation of an ideal state. The result is also a fractional power law (41), giving an ω^m behavior for the susceptibility function. Once again the value of m is in the range $0 < m < 1$, and m represents the degree of structural order, this time on the larger scale of the cluster, i.e., the degree of ordering in the cluster array. Hence, $m \rightarrow 0$ indicates an almost ideal lattice structure, whereas $m \rightarrow 1$ may give rise to a wide distribution of clusters. The intracuster motion and the intercluster exchange mechanisms are schematically represented in the Fig. 8 (28).

For the intracluster motion the susceptibility function is given by (41)

$$\chi(\omega) \propto \left(1 + i \frac{\omega}{\omega_p}\right)^{1-n} {}_2F_1\left(1-n, 1 - m \frac{\omega_p}{\omega_p + i\omega}\right) \quad (82)$$

where ${}_2F_1$ is the Gaussian hypergeometric function. It should be noted that the asymptotic limits of Eq. (82) are the universal relaxation law [i.e., Eqs. ((69)) and ((70))] (8).

The Dissado–Hill quantum-mechanical model (41) describes a *QDC* phenomenon as a partial conduction process that is equivalent to the *LFD* phenomenon (8) described above. In the *QDC* process similar considerations to those for the dipoles are given to systems containing charge carriers. The difference between a *QDC* process and dc conduction at low frequencies is that the latter phenomenon is characterized by

$$\chi(\omega) \rightarrow \text{constant} \quad (83)$$

and

$$\chi''(\omega) \propto \frac{\sigma_{dc}}{\omega} \quad (84)$$

where σ_{dc} is the frequency-independent dc conductivity. For the high frequencies, the Maxwell–Wagner interfacial polarization effect (1) may be used to predict a limiting behavior of the form

$$\chi'(\omega) \propto \omega^{-2} \quad (85)$$

$$\chi''(\omega) \propto \omega^{-1} \quad (86)$$

and

$$\chi''(\omega)/\chi'(\omega) \propto \omega \quad (87)$$

The Dissado–Hill model (41) suggests that the motion of all charge carriers within a cluster of correlation length is cooperative, i.e., the motion of a charge carrier to a neighboring site is limited to the vacancy of such sites and by other charges surrounding it. The model (41) divides the response into high-frequency (short-time) behavior above a critical frequency ω_c , where intracluster motion occurs, and low-frequency (long-time) behavior below ω_c , where intracluster motion exchange occurs. The intracluster motion, which is analogous to the flipping of dipoles, is now replaced by the hopping of charges between available sites within a correlation length ξ , which reduces the overall polarization of the cluster. The high-frequency response has the same functional form as for the dipoles, i.e., ω^{n-1} , $0 < n < 1$. Again the physical meaning of the exponent n is the average degree of structural ordering within a cluster, and small values of n will correspond to irregularities in a cluster such as might occur when an interstitial ion or a dislocation is present. The parameter n may also be related to the entropy density per cluster constituent. The value of n may be independent of temperature for thermally stable cluster structuring (41).

In the intercluster exchange there is a physical transport of charges between the clusters. The charge motion is no longer correlated with the available sites of the donor cluster, but rather with those of the acceptor cluster. For this case the susceptibility function is shown to be a fractional power law of the form ω^{-p} , with

26 DIELECTRIC PERMITTIVITY AND LOSS

$0 < p < 1$ (41). A small value of p indicates a set of clusters that are almost identical to each other, whilst a large value of p is associated with a broader distribution of clusters in which intercluster exchanges can carry the effective charge through many clusters over a long distance. In the presence of both the intracluster hopping and intercluster charge transport, the susceptibility function of the system is given by (42)

$$\chi(\omega) \propto \left(\frac{\omega_c}{\omega_c + i\omega} \right)^{1-n} {}_2F_1 \left(1-n, 1+p, 2-n; \frac{\omega_c}{\omega_c + i\omega} \right) \quad (88)$$

The asymptotic forms of $\chi(\omega)$ at high and low frequencies with respect to ω_c are (42)

$$\chi'(\omega) \propto \chi''(\omega) \approx \chi'(\omega_c)(\omega/\omega_c)^{-p} \quad \text{for } \omega \ll \omega_c \quad (89)$$

$$\chi'(\omega) \propto \chi''(\omega) \propto \chi'(\omega_c)(\omega/\omega_c)^{n-1} \quad \text{for } \omega > \omega_c \quad (90)$$

Once again, it may be noted that the asymptotic values of this model (41,42) are the same as those of the universal-law model (8,15). The relations between the exponents n and p of these two models are

$$p = 1 - n_2 \quad (91)$$

$$n = n_1 \quad (92)$$

where n_1 and n_2 refer to the values of the parameters of the universal law above and below ω_c , respectively (41), i.e.,

$$\chi'(\omega) \propto \chi''(\omega) \propto \omega^{n_2-1} \quad \text{for } \omega \ll \omega_c \quad (93)$$

$$\chi'(\omega) \propto \chi''(\omega) \propto \omega^{n_1-1} \quad \text{for } \omega > \omega_c \quad (94)$$

Summarizing the above, it appears that all dielectric materials commonly investigated have the following characteristics in terms of the indices n and m (41):

- (1) $n = 0, m = 1$ express the Debye limit of an ideal liquid with independent cluster constituents in the system.
- (2) $n = 1, m = 0$ occurs in an ideal crystal with no internal relaxation and zero loss.
- (3) For real liquids $n \rightarrow 0, m \rightarrow 1$, and the average clusters are weakly bound.
- (4) For plastic crystals, waxes, and viscous liquids, $n \approx 1/2$ and $m \approx 1/2$. These materials have clusters with restricted structural range.
- (5) For solids with interstitial impurities and ferroelectrics, $n \rightarrow 0$ and $m \rightarrow 1$. Ferroelectrics have weakly bound clusters of dipole reversals, thus yielding a small value of n .

Table 9: Theoretical Concepts of Relaxation Models (29, 36)

Function	Equation	Parameters
Debye	$\chi''(\omega) \propto \frac{1}{(\omega/\omega_p)^{-1} + (\omega/\omega_p)}$ (26)	$\alpha = 0, \quad \beta = 1$
Cole–Cole	$\chi''(\omega) \propto \frac{1}{(\omega/\omega_p)^{\alpha-1} + (\omega/\omega_p)^{1-\alpha}}$ (27)	$0 < \alpha < 1, \quad \beta = 1$
Davidson–Cole	$\chi''(\omega) \propto \frac{1}{(\omega/\omega_p)^{-1} + (\omega/\omega_p)^\beta}$ (28)	$\alpha = 0, \quad 0 < \beta < 1$
Havriliak–Negami	$\chi''(\omega) \propto \frac{1}{(\omega/\omega_p)^{\alpha-1} + (\omega/\omega_p)^{\beta(1-\alpha)}}$ (29)	$0 < \alpha < 1, \quad 0 < \beta < 1$
Jonscher, Dissado, and Hill (dipolar peak)	$\chi''(\omega) \propto \frac{1}{(\omega/\omega_p)^{-m} + (\omega/\omega_p)^{n-1}}$ (21)	$0 < m < 1, \quad 0 < n < 1$
Jonscher, Dissado, and Hill (QDC process)	$\chi'(\omega) \propto \chi''(\omega) \propto \omega^{n_2-1}$ for $\omega \ll \omega_c$ (24) $\chi'(\omega) \propto \chi''(\omega) \propto \omega^{n_1-1}$ for $\omega \gg \omega_c$ (25)	$0 < n_2 < 1, \quad 0 < n_1 < 1$
Weron (stochastic model)	$\phi(t) = \phi_0 \alpha \omega_p (\omega_p t)^{\alpha-1} [1 + k(\omega_p t)^\alpha]^{-(1+k)/k}$ (41)	$m = \frac{1-n}{k}, \quad 1 - n < m < 1$

(6) For imperfectly crystallized materials with topographical impurities, glasses, and vitreous polymer systems, $n \rightarrow 1$ and $m \rightarrow 0$.

It may be noted that $n + m = 1$ will only occur when the intra- and intercluster displacements lie along the same coordinates, i.e., in Lennard–Jones liquids (43) and hydrogen-bonded systems (44).

The cluster model (41,42) is in many ways the most rigorous description of relaxation of defects in a dielectric system, and it offers an *ab initio* derivation of the entire spectral shape of the frequency dependence of the susceptibility function.

Table 9 lists the theoretical concepts of dielectric relaxation models, discussed above.

Electric Equivalent Circuits for Dielectric Loss. A dielectric capacitor can be represented by an electrical circuit where the dielectric loss is reproduced mainly by an equivalent resistance R in series or in parallel with the capacitor and, occasionally, an inductance. A Debye system can be represented, for example, by a resistance and a capacitance in series, whilst non-Debye behavior of dielectric susceptibility may be constructed with more complex circuits.

For such cases, the concept of a *universal* capacitor (8) has been proposed, and the resulting frequency dependence of the dielectric parameters is

$$\chi(\omega) \propto C_n(\omega) = \beta(i\omega)^{n-1} = \beta \left(\sin \frac{n\pi}{2} - i \cos \frac{n\pi}{2} \right) \omega^{n-1} \quad (95)$$

It should be noted that for nonideal dielectric responses, the circuit elements will have frequency-dependent dispersive properties. Figure 9 shows schematic representations of simple circuit combinations

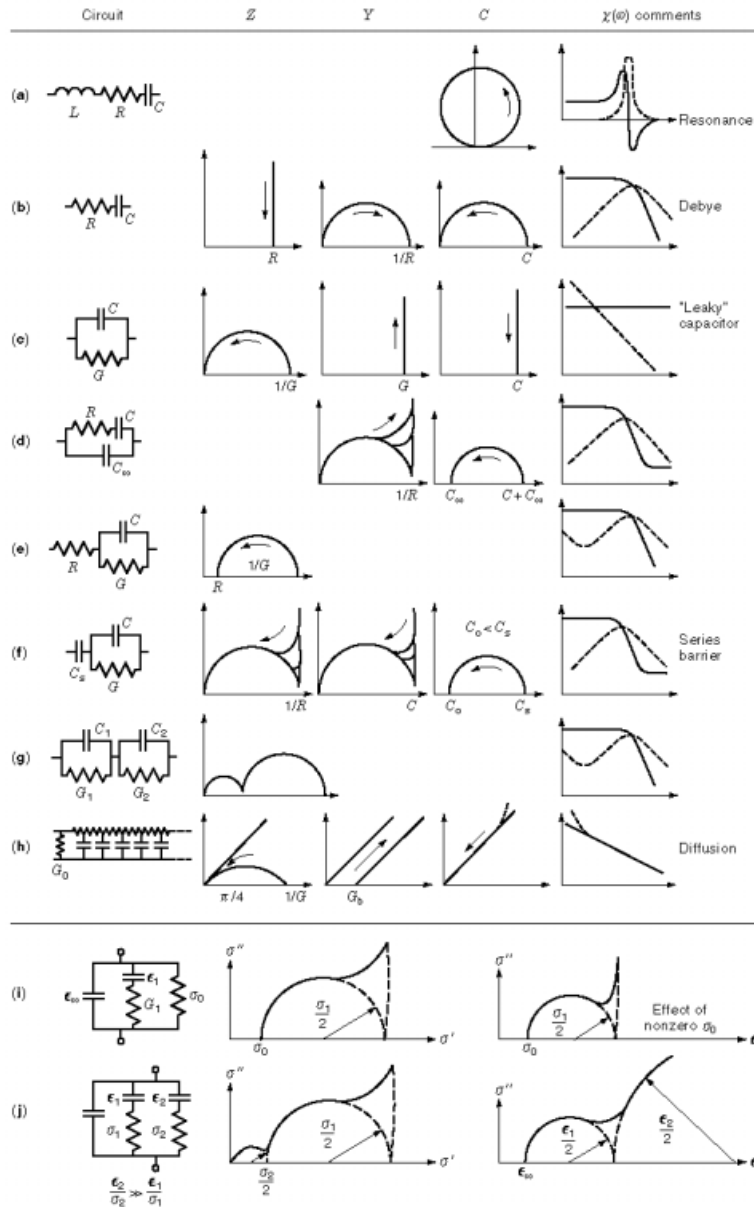


Fig. 9. Schematic representation of simple circuits formed as a combination of ideal, frequency-independent elements (a–h), and some forms of presentation of dielectric data (i, j) (8,36,45).

of ideal, frequency-independent elements and some forms of presentation of dielectric data. The frequency response of lossy capacitors of the type represented by Eq. (89) is shown in Fig. 10 (8,36,45). The association of universal capacitors and dispersive circuit elements is schematically represented in Table 10 (29).

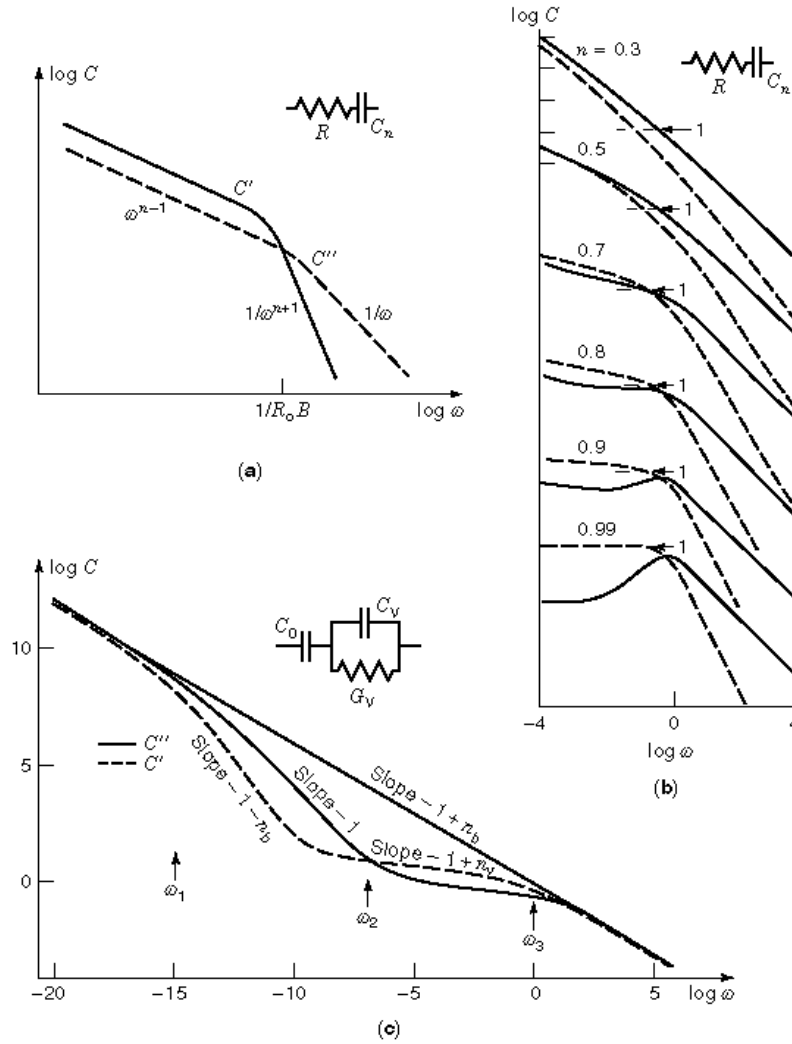


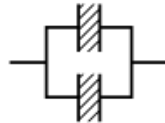



Fig. 10. The frequency response of circuits involving universal lossy capacitors of the type $C_n = B (i\omega)^{n-1}$: (a) response of a series combination of C_n with a resistor R ; (b) calculated frequency dependences for a range of values of the exponent n ; (c) the response of the series-parallel circuit shown, with two universal capacitors, one of which corresponds to a series barrier region, while the other forms the equivalent of a volume region with its parallel conductance G_v . The values of parameters assumed in the calculation are as follows: $B_v = 1$, $G_v = 10^{-6}$, $n_v = 0.85$, $B_s = 1$, $n_s = 0.4$. At very low frequencies the volume behavior is dominated by the conductance, and the response is that of a series combination of C_b and G_v , which is therefore closely similar to that seen in (a) (8).

Relaxation Behavior in Materials. The relaxation phenomena have been studied for a wide range of materials, from covalent, ionic, and van der Waals crystals at one extreme through glasses, liquids containing suspensions, solid synthetic polymers, and p - n junctions at the other (41).

The permittivity of nonpolar gases at normal pressure is close to unity, and the Clausius-Mossotti equation (23) adequately describes its variation with moderate density changes (46). At high pressures the molar

Table 10: Electrical Analog Equivalent Circuits (29)

Circuit	Function
	Debye (Equation 52)
	Dipolar relaxation (Equation 67)
	QDC process (Equations 87 and 88)
	Flat loss (Equation 87)

polarization of gases deviates from the Clausius–Mossotti equation. The molecular polarizability is enhanced by the attractive forces between the molecules, whereas the repulsive forces decrease it.

Centrosymmetric molecules do not possess dipole or octupole moments, but quadrupole moments may be present in some gases, e.g., hydrogen, carbon dioxide, carbon disulfide, oxygen, nitrogen, benzene, and ethylene. Tetrahedral molecules, on the other hand, have zero dipole and quadrupole moments (e.g., methane and carbon tetrachloride) (46). The presence of higher dipole moments in a molecule induces moments on its neighbors and produces deviations from the Clausius–Mossotti equation. Polar gases display temperature dependence of the orientational polarization, and their dielectric loss spectra follow the Debye relaxation behavior in which partial orientation of the permanent dipoles occurs under an externally applied field. Polar gases absorb energy in the microwave region through two processes: rotational absorption and unquantized molecular collision. The high-frequency dielectric properties of gases have been well reviewed (47,48) and will not be discussed further here.

There is as yet no exact theory of liquids, which have been treated either as dense gases or as disordered solids. The dielectric relaxation in polar liquids (dilute solutions) with spherical dipolar molecules can be interpreted in terms of the orientation of individual dipoles. In the Debye process, it is assumed that a spherical dipolar molecule obeys Stokes's law, which states that the relaxation time is proportional to the shear viscosity of the liquid and to r^3 , where r is the radius of the sphere. However, the relaxation time must depend on the viscosities of both the solvent and the solute. The molecular radius calculated from the relaxation time with the Debye model is usually too small. Improved fit to the relaxation behavior of liquids may be obtained with empirical formulae [Cole–Cole (20), Davidson–Cole (21), Havriliak–Negami (23,24)] and the universal law (8).

The intermolecular forces in associated liquids are stronger and perhaps more directional in some cases than in other liquids. Water is probably the most important associated liquid. The dielectric relaxation behavior

of water agrees well with the Cole–Cole model (20) with $\alpha = 0.02 \pm 0.007$ (45,49). It has been suggested (50) that the kinetic process responsible for the dielectric relaxation in water is cluster formation. Water is composed of fluctuating clusters of bonded molecules with unbonded molecules between them. Individual molecules are able to move frequently from one cluster to another, and their dipole orientation will depend on the number of hydrogen bonds they form (45,50). It should be noted that the clustering is a random process and that it is not possible to subdivide water molecules into groups that remain the same over a period of time longer than the average relaxation time, $\approx 9.6 \times 10^{-12}$ s, which is perhaps related to the OH stretching vibration at 1.10×10^{13} Hz. This vibration is affected by the hydrogen bonding. Alcohols have a wide distribution of relaxation times, which tend to follow the empirical Cole–Cole (20) and Davidson–Cole (21) models. The dielectric properties of liquids have been well reviewed elsewhere (45,50) and will not be discussed further here.

A perfect alkali halide ionic crystal such as NaCl can only be polarized by perturbing its thermal vibrations. However, in practice all crystals contain dislocations, i.e., polarizable flaws, which do not always distort the lattice, particularly when the ionic radii are similar (45). The dielectric relaxation behavior in such materials is complicated by the presence of their ionic and electronic conductivities. For these materials the relaxation time τ tends to be long (≈ 1 s) at room temperature, and it obeys

$$\tau = Ae^{E_a/kT} \quad (96)$$

where E_a is the thermal activation energy and A is a constant. It is of interest to note that the mechanical relaxation time of these materials is often half the dielectric one, neglecting electrostatic interactions. This implies that the shear modes of polarization relax twice as fast as the tensile ones (45). The dielectric behavior of alkali halides with divalent cations has been reviewed extensively by Meakins (51).

Organic semicrystalline and amorphous polymers are practical electrical insulating materials that consist of macromolecules. Such molecular solids have both covalent and van der Waals bonds, which make the molecular motions easy in comparison with entirely covalently bonded solid dielectrics. The activation process in these materials also follows an Arrhenius relationship of the form of Eq. (90) except at the glass transition temperature T_g . The relaxation process at T_g is approximated by the William–Landel–Ferry relationship (52),

$$\tau(T) = \tau_0 \exp\left(\frac{C_1(T - T_g)}{C_2 + T - T_g}\right) \quad (97)$$

where τ_0 is a constant, and C_1 and C_2 are also constants with values ≈ 17 and ≈ 51 respectively (46). The relaxation time τ decreases with increasing temperature, as may be observed in isochronal plots of depolarizing current against temperature (53).

The relaxation behavior of polymers is related to several complex physical parameters, viz., shear modulus, heat capacity, permittivity, and refractive index, which exhibit transitions with increasing temperature (54) (see Fig. 11). In an amorphous polymer the principal transition is the glass transition at a temperature T_g , which is labeled as the α -transition at T_α in Fig. 11. Above T_g the free volume decreases to a critical value, thus severely restricting the segmental motions of the polymer chains. In a semicrystalline polymer there will be an additional transitional phenomenon at the melting temperature T_m . There are other secondary transitions, β and γ in order of decreasing temperature, i.e., $T_\alpha > T_\beta > T_\gamma$. For example, in polyethylene, the α , β , and γ relaxations at 1 kHz occur at 77° , -13° , and -113°C , respectively. The α relaxation is attributed to motions in the crystalline phase, and the β relaxation arises from primary motions of the chain branches in the amorphous phase. The γ relaxation may be associated with a combination of processes including defect migration and the reorientation motion in the amorphous phase (55). The α , β , and γ relaxations in polypropylene occur at 80° , 0° , and -80°C . Table 11 gives the glass transition temperatures T_g of some common polymers (54).

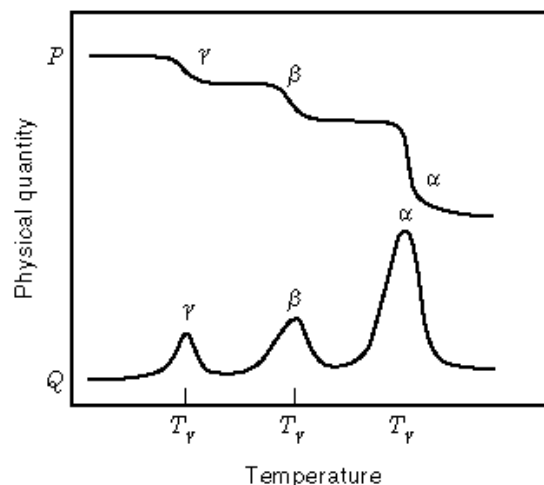


Fig. 11. Schematic diagram of the temperature dependence of complex properties of polymers (54).

Experimental Evidence of Frequency Response and a Comparison with the Cluster Models.

Although ideal Debye response in ferroelectric single crystals has been observed (56), there exist, in general, very few examples of such responses in condensed matter. Although water may be regarded as a classic dielectric, its dielectric behavior displays a broadened relaxation peak that departs from a true Debye relation (8,57). Near-Debye relaxation responses have also been observed in silicon p - n junctions (8). It may not be appropriate to discuss experimentally observed dielectric dispersion data with the Cole–Cole, Davidson–Cole, and Havriliak–Negami models, which are basically empirical in nature. However, relaxation spectroscopy can provide considerable information on dielectric materials from the measurement of the shape of the loss peak as well as the relaxation rate and amplitude. The shape of a loss peak is clearly characterized by the parameters m and n of the Dissado–Hill (41,42) and Universal-law (8) models. This procedure has been employed to demonstrate the presence of cluster structure in (i) the viscous liquid produced from the glassy state above a glass transition (58), (ii) plastic crystal phases (59), and (iii) ferroelectrics (60,61). The cluster size becomes strongly temperature-dependent in ferroelectrics near the Curie temperature (61). The amplitude and the relaxation rate are related (60,61,62). The above considerations also hold true for liquid crystals (60,61,63). Figure 12(a) and 12(b) show the observed dielectric response of poly-*r*-benzyl-L-glutamate (*PBLG*) and poly-*r*-methyl-L-glutamate (*PMLG*), respectively (42). The loss peaks in both cases are broad with values of n and m in conformity with the cluster model (41). Table 12 gives the values of shape indices n and m for *PBLG* in different states, from which it may be observed that as the local order decreases in solution the value of n decreases, and that of m increases (41,63). These examples cover some typical cluster structures with different values of m and n (41).

It is suggested that the quantum-mechanical cluster model provides explanations for the relaxation dynamics in materials that show non-Debye susceptibility behavior over a wide frequency range. The cluster model shows that the free energy of a cluster is held constant and its entropy evolves at the expense of its internal energy (i.e., enthalpy), resulting in a power-law relaxation process.

Table 11: Glass Transition Temperature T_g of Common Polymers^a (54)

Polymer	T_g ($^{\circ}\text{C}$)
PE	-90, -35
PP	-10
Polymethylpentene	30
PS	95
PAN	105
PVC	85
PVF	-20, 45
PVDC	-15
PA 6	50
PA 66	90
PA 610	40
PMMA	105
POM	-90, -10
Poly (phenylene oxide)	210
PC	150
PETP	65
CA	105
NR	-75
CR	-45
NBR	-20

^aThese are approximate values; where two temperatures are given, the assignment of the glass transition remains doubtful. T_m is independent of chain length for high-molar-mass polymers, but falls somewhat as the chains become very short.

Application of Dielectric Spectroscopy in Detecting Aging In Insulating Polymers

Dielectric Aging and Treeing. Polymers experience aging when subjected to a mechanical or electric stress over an extended period of time. The aging produces irreversible deterioration of physical, chemical, and dielectric and other electrical properties, which may eventually lead to electrical breakdown of an insulating polymer. It must be stressed that physical and chemical aging may occur independently without the application of an external electric field. However, the aging process may be accelerated by the field in conjunction with other factors.

The mechanisms for electrical breakdown have been extensively reviewed in recent years (64). The chemical aging models have also been reviewed (65) and will not be discussed in detail here. The present section provides in brief the results of a study of aging of polyethylene under an ac field in humid environment by dielectric spectroscopy.

Dielectric aging in dry environment at moderate to high electric field appears to begin mostly at imperfections in materials where the local field tends to be enhanced. At such locations, treelike electrical channels may form and propagate due to the occurrence of partial discharges. Space charges play a significant role in the initiation and growth of electrical trees (66). Water trees in polymeric insulators with ac fields in humid environment may arise from microphase separation in partially oxidized polymers as a result of field-induced electrochemical processes (67). It has been shown that water trees in cross-linked polyethylene consist of tracks of hydrophilic carboxylate salts in the amorphous phase of the polymer (68,69,70). The dielectric aging and the

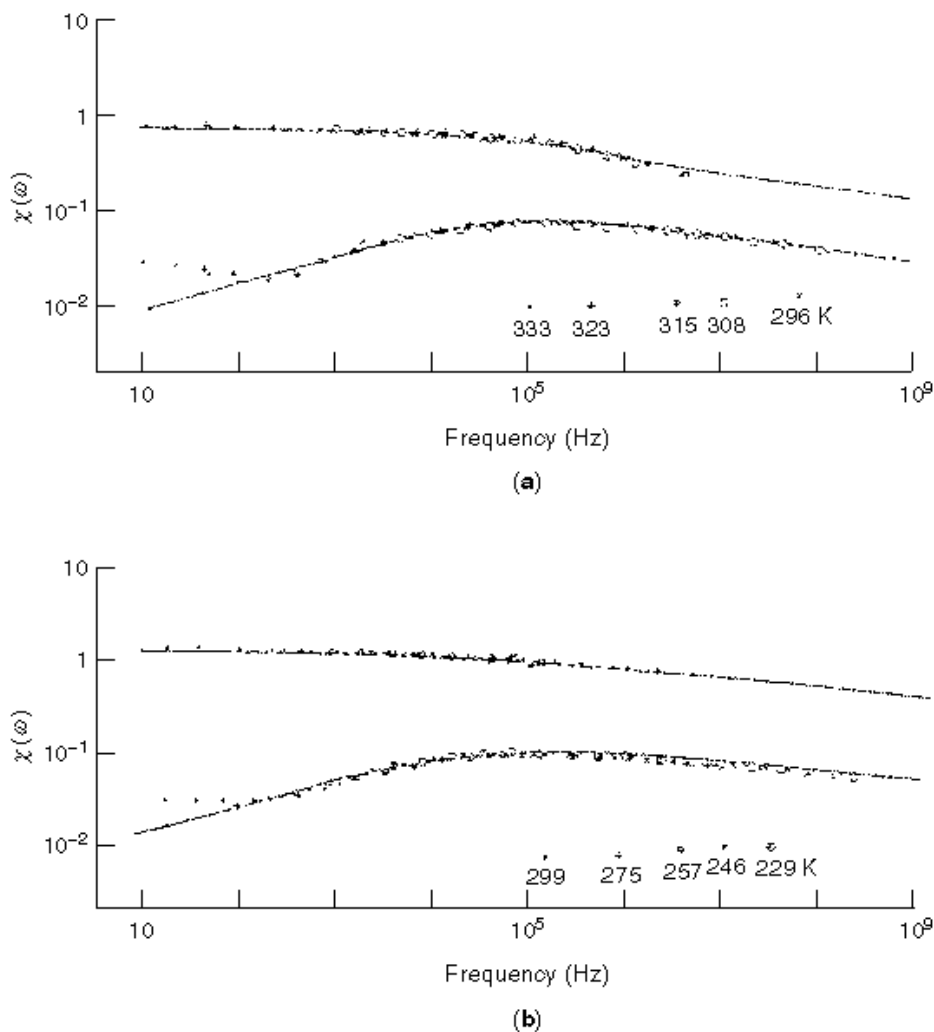


Fig. 12. Master curves for the dielectric response of oriented films of (a) *PBLG* and (b) *PMLG*. The theoretical spectral shape in the plots has been determined with the values (a) $m = 0.28$, $n = 0.87$; (b) $m = 0.24$, $n = 0.92$. Plot (a) is scaled at 333 K, and (b) at 299 K. In both, the small magnitude of the dispersion has limited the accuracy with which the real part of the susceptibility could be determined for the higher frequency values (42).

water-tree growth incorporate electrochemical processes following the electrophysical process of water and ion diffusion in the polymer (68). It has been suggested that the electrochemical degradation of polyolefins associated with aging and water treeing involve five fundamental steps: (i) electrolysis of water, in which oxygen and hydrogen peroxide radicals are formed, both being oxidizing agents, (ii) initiation of degradation, (iii) catalysis of degradation by metal ions, (iv) chain scission, resulting in the formation of ketones and carboxylate ions, and (v) conversion of ketones to carboxylate ions (71). Electric-field-driven oxidation has also been proposed by other workers (64,72,73,74).

The electrooxidation occurs in the local field direction, and water-tree tracks are formed by chain scission in the amorphous regions of the polymer. The track region is hydrophilic. As a result, water molecules in

Table 12: The Spectral Shape Indices Observed in the Dielectric Response of PBLG in Different Physical States (41, 63)

Sample	m	n
Solid, orientationally ordered film	0.28	0.87
Solid, prepared by the Leuch method	0.42	0.81
Solution in benzene with ϵ -caprolactam	0.78	0.50
Solution in <i>trans</i> -1,2-dichloroethylene containing <i>NN</i> -formidemethylamide	1.0	0.50
Solution in purified ethylene dichloride	0.78	0.49
Solution in ethylene dichloride	0.61	0.49
Solution in dioxan	—	0.44
Solution in dioxan with DMF	0.76	0.51
Solution in dioxan	0.81	0.54

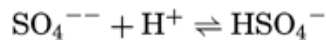
the polymer matrix condense to form liquid water in the track, which then transports ions to provide further oxidation at the tip of the track. Thus a track propagates itself in a similar manner to that of a self-propagating electrical tree or a gas breakdown channel, although at a different rate (71).

It may thus be expected that aging and its progress due to the electrooxidation of a polymer in a humid environment may be detected by a study of its dielectric behavior over a wide frequency range.

Evidence of Aging in Frequency Response. Figure 13 shows the frequency response of the real and the imaginary parts [$\chi'(\omega)$ and $\chi''(\omega)$, respectively] of the complex susceptibility $\chi(\omega)$ of unaged and cross-linked polyethylene (*XLPE*) cable samples and samples ac-aged (6 kV/mm, 50 Hz) for up to 6000 h in water at room temperature (36,75). It may be observed from the fitted response that there are three relaxation processes: (i) a high-frequency (*HF*) loss peak at $\sim 5 \times 10^5$ Hz, (ii) a medium-frequency (*MF*) loss peak at ~ 1 Hz, and (iii) a low-frequency (*LF*) loss peak at $\sim 10^{-4}$ Hz. It is suggested that the *HF* loss peak is due to bound water containing ions. It has been stated that in principle there are two relaxations in water: the fluctuations in polarization and the dissociation of water into ions. The latter relaxation occurs in the gigahertz range, whereas the former one may be observed at $\sim 10^5$ Hz. For example, for a solution of MgSO_4 in water at 20°C (76), the following chemical reactions of the electrolyte may occur, each possessing its own relaxation characteristic:



and



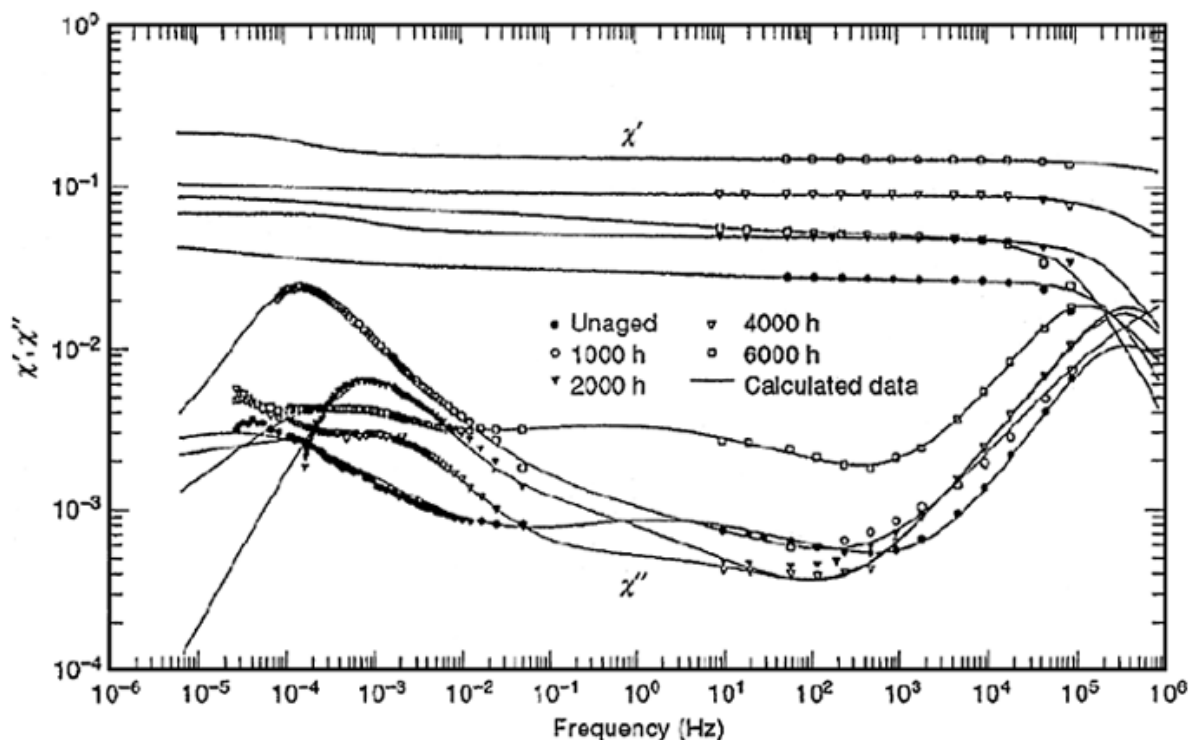


Fig. 13. Dielectric behavior of *XLPE* cable samples, unaged and ac-aged ($6 \times 10^6 \text{ V}\cdot\text{m}^{-1}$, 50 Hz, room temperature, water) up to 6000 h (36).

The first process is slower than the second, for which the relaxation peak occurs at $\sim 2 \times 10^5 \text{ Hz}$, which is in agreement with the location of the *HF* peak in Fig. 13 (45,76). The second chemical reaction is more rapid and is outside the experimental range of Fig. 13. The *HF* peak (Fig. 13) is observed to be fairly independent of the aging time. It has also been shown that the diffusion coefficient of water vapor in polyethylene is $\approx 1.4 \times 10^{-6} \text{ m}^2/\text{s}$ and is independent of electrical stress (77,78). Furthermore, polar impurities in polyethylene have been alleged to attract water (70), which will be bound in the polymer. In view of the above observations, the origin of the observed *HF* peak (Fig. 13) may be attributed to the ions in bound water, as stated before (28,29,36).

XLPE cable samples contain cross-linking by-products (such as cumyl alcohol and acetophenon, as well as antioxidants), which may diffuse out of the cable with the progress of time. In addition, antioxidants react chemically with the oxidation products in the sample. The *MF* loss peak at $\sim 1 \text{ Hz}$ appears to increase slightly (Fig. 13) with continued aging. It also becomes broader, overlapping with the *LF* peak. It is suggested that the *MF* peak may originate from the presence of the polar moieties discussed above (28,29,36).

The *LF* loss peak (Fig. 13), occurring at 10^{-4} Hz , changes significantly with aging. It may be noticed that the magnitude of this peak at first rises sharply, up to an aging time of 1000 h. Subsequently it decreases progressively, although its magnitude is still greater after 6000 h of aging than that of the unaged sample. Furthermore, the *LF* loss peak becomes broader with increasing aging time.

The *LF* loss peak amplitude increases initially because of the formation of free radicals. It may be argued that a competitive process involving the production of polar moieties due to electrochemical reactions and

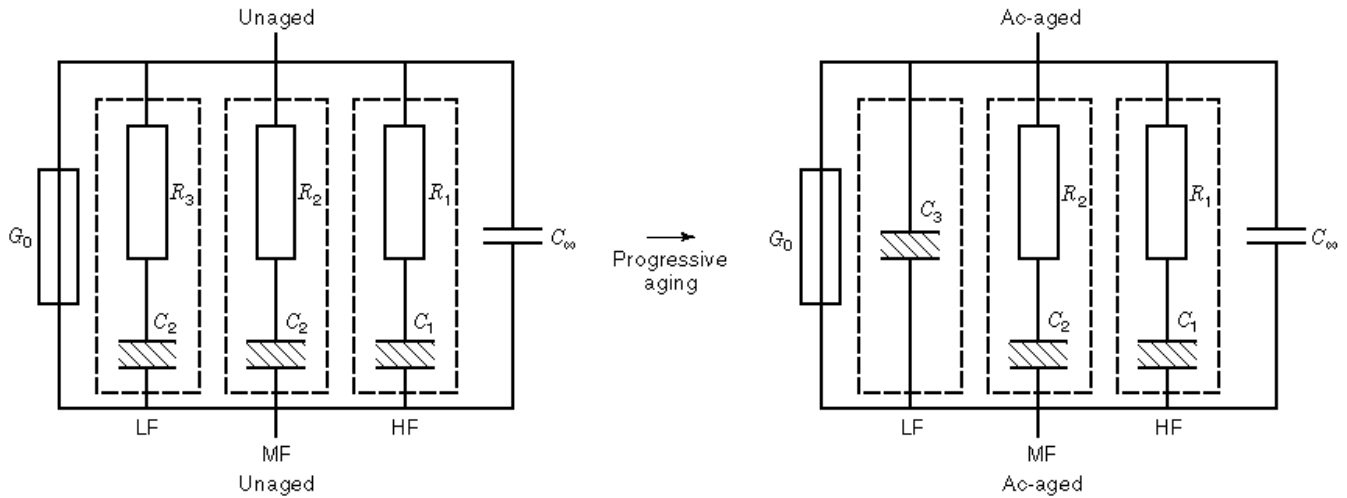


Fig. 14. Analog equivalent circuits of unaged and ac-aged *XLPE* cable samples (28,36,75).

injected space charges establishes itself with increasing aging time. Eventually, the space-charge component becomes dominant as the polymer becomes more conductive. The relaxation loss behavior thus shows the presence of intracuster interaction in the *MF* to *HF* region and of intercluster charge motion in the low-frequency region, the latter phenomenon becoming dominant with continued aging (29,36).

Figure 14 (28,36,75) shows a possible electrical equivalent circuit for the unaged and electrically aged *XLPE* samples in a humid environment. The dielectric relaxation behavior of the unaged *XLPE* cable sample of Fig. 13 may be represented by a parallel-connected network of (i) three series-connected frequency-dependent resistances R_1 , R_2 , and R_3 and (ii) three dissipative capacitances C_1 , C_2 , and C_3 , giving three dipolar peaks in the *LF*, *MF*, and *HF* regions. The *QDC* response in the *LF* region with progressive aging has been taken into account by removing the resistance R_3 from the circuit. The observed broadening of the *MF* peak with aging will cause R_2 to diminish with aging, although it will still have a nonzero value. The values of R_1 and C_1 for the *HF* peak should not change significantly, as the *HF* peak remains unaffected by field aging. Figure 14 also incorporates the very high-frequency capacitance C_∞ and G_0 in parallel. The latter parameter represents any dc conduction mechanism in the dielectric (75).

It is thus suggested that the dielectric spectroscopy, particularly in the *LF* range, may be a convenient tool in identifying aging (79). Furthermore, the Debye relaxation model (3) and the intracuster and intercluster many-body interaction model (41,42) may provide explanations for the observed relaxation behavior at a molecular level.

BIBLIOGRAPHY

1. C. J. F. Böttcher P. Bordewijk *Theory of Electric Polarization*, 2nd ed., Vol. 1, Amsterdam: Elsevier, Chaps. 1, 2, pp. 9–90. 1973.
2. H. Fröhlich *Theory of Dielectric Constant and Dielectric Loss*, Oxford: Clarendon, 1958, Chap. 1, pp. 1–14.
3. P. Debye *Polar Molecules*, New York: Dover, 1929, Chap. 5.
4. A. A. Zaky R. Hawley *Dielectric Solids*, London: Routledge, Kegan & Paul, 1970, Chaps. 1, 2, pp. 2–25.
5. A. R. Von Hippel (ed.) *Dielectric Materials and Applications*, Cambridge, MA: MIT Press, 1954, Chaps. 1–3, pp. 3–36.

38 DIELECTRIC PERMITTIVITY AND LOSS

6. M. C. Lovell A. J. Avery M. E. Vernon *Physical Properties of Materials*, New York: Van Nostrand-Reinhold, 1976, Chap. 8, pp. 153–184.
7. A. Schönhal Dielectric properties of amorphous polymers, in J. P. Runt and J. J. Fitzgerald (eds.), *Dielectric Spectroscopy of Polymer Materials*, Washington: Amer. Chem. Soc., 1997, Chap. 3, pp. 81–106.
8. A. K. Jonscher *Dielectric Relaxation in Solids*, London: Chelsea Dielectric Press, 1983, Chap. 2, pp. 13–61.
9. C. A. West R. M. Thomson *Physics of Solids*, New York: McGraw-Hill, 1970, Chaps. 18, 19, pp. 388–421.
10. R. Sanger O. Steiger K. Gachter Temperatureeffect der Molekularpolarisation einiger Gase und Dampfe, *Helv. Phys. Acta*, **5**: 200–210, 1932.
11. C. Smyth W. Walls Dielectric investigation of nitromethane and chloropicrid, *J. Chem. Phys.*, **3**, 557–559, 1935.
12. C. Smyth C. Hitchcock Dipole rotation and the transition in the crystalline hydrogen halides, *J. Am. Chem. Soc.*, **55**: 1830–1840, 1933.
13. J. C. Anderson *Dielectrics*, London: Chapman & Hall, 1964, Chap. 7, pp. 83–97.
14. L. Hartshorn J. A. Saxton *Handb. Phys.*, **26**: 640, 1958.
15. G. Williams D. C. Watts Non-symmetrical aspects of multiple dielectric relaxation in behaviour arising from a single empirical decay function, *Trans. Faraday Soc.*, **66**: 80–85, 1970.
16. A. K. Jonscher *Universal Relaxation Law*, London: Chelsea Dielectric Press, 1996, Chap. 1, pp. 1–44.
17. J. M. Alison A dielectric study of lossy materials over the frequency range of 4-82 GHz, PhD Thesis, University of London, 1990.
18. R. M. Hill A. K. Jonscher *The dielectric behaviour of condensed matter and many body interpretation*, *Contemp. Phys.*, **24**: 75–110, 1983.
19. J. M. Alison R. J. Sheppard A precision wave-guide system for the measurement of complex permittivity of lossy liquids and solid tissues in the frequency range 29 GHz–90 GHz, 1: The liquid system for 29–45 GHz—an investigation in water, *Meas. Sci. Technol.*, **1**: 1093–1098, 1993.
20. K. S. Cole R. H. Cole Dispersion and absorption in dielectrics, 1. Alternating current characteristics, *J. Chem. Phys.*, **9**: 341–351, 1941.
21. D. W. Davidson R. H. Cole Dielectric relaxation in glycerol, propylene, and *n*-propanol, *J. Chem. Phys.*, **12**: 1484–1490, 1951.
22. R. M. Fuoss J. G. Kirkwood Electrical properties of solids. VIII. Dipole moments in polyvinyl chloride diphenyl systems, *J. Amer. Chem. Soc.*, **63**: 385–394, 1941.
23. S. Havriliak S. Negami A complex plane analysis of α -dispersion in some polymer systems, *J. Polym. Sci C*, **14**: 99–117, 1966.
24. S. Havriliak S. Negami A complex plane representation of dielectric and mechanical relaxation processes in some polymers, *Polymer*, **8**: 161–210, 1967.
25. J. R. Macdonald Transient and temperature response of a distributed, thermally activated system, *J. Appl. Phys.*, **34**: 538–552, 1963.
26. B. Gross Electret research—stages in development, *IEEE Trans. Electr. Insul.*, **EI-21**(3): 249–269, 1986.
27. B. Gross Distribution functions in linear viscoelastic theory, *J. Appl. Phys.*, **62**: 2763–2770, 1987.
28. D. K. Das-Gupta P. C. N. Scarpa Polarization and dielectric behaviour of ac-aged polyethylene, *IEEE Trans. Dielectrics Electr. Insul.*, **3**: 366–374, 1996.
29. D. K. Das-Gupta P. C. N. Scarpa Modelling of dielectric relaxation spectra of polymers in the condensed phase, *IEEE Electr. Insul. Mag.*, **15**: 23–32, 1999.
30. G. C. Garton The distribution of relaxation times in dielectrics, *Trans. Faraday Soc. A*, **42**: 55–60, 1946.
31. N. G. McCrum B. E. Read G. Williams Phenomenological theories of mechanical and dielectric relaxations, in *Anelastic and Dielectric Effects in Polymer Solids*, New York: Wiley, 1967, Chap. 4, pp. 102–237.
32. C. J. Dias Determination of a distribution relaxation frequency, *Phys. Rev. B*, **53**: 14212–14222, 1996.
33. K. Liedermann The calculation of a distribution of relaxation times from the frequency dependence of the real permittivity with the inverse Fourier transformation, *J. Non-cryst. Solids*, **175**: 21–30, 1994.
34. A. K. Jonscher Dielectric response of polar materials, *IEEE Trans. Electr. Insul.*, **25**: 622–629, 1990.
35. A. K. Jonscher The universal dielectric response and its physical significance, *IEEE Trans. Electr. Insul.*, **EI-19**: 567–577, 1992.
36. P. C. N. Scarpa Polarization and dielectric behaviour of ac aged polyethylene, PhD Thesis, University of Wales, 1995.

37. K. Weron A probabilistic mechanism hidden behind the universal power law for dielectric relaxation, *J. Phys. Condensed Matter*, **3**: 9151–9162, 1991.
38. K. Weron A. Jurlewicz Two forms of self-similarity as a fundamental feature of the power-law dielectric response, *J. Phys. A Math. Gen.*, **26**: 395–410, 1993.
39. A. Weron K. Weron W. A. Wyoczynski Relaxation functions in dipolar materials, *J. Statist. Phys.*, **78**: 1027–1038, 1995.
40. J. T. Bender M. F. Shlesinger Derivation of the Kohlrausch–Williams/Watts decay law from activation energy dispersion, *Macromolecules*, **18**: 591–592, 1985.
41. L. A. Dissado R. M. Hill A cluster approach to the structure of imperfect materials and their relaxation spectroscopy, *Proc. Roy. Soc. London*, **390**: 131–180, 1983.
42. L. A. Dissado R. M. Hill Anomalous low frequency dispersion, *J. Chem. Soc. Faraday Trans. 2*, **80**: 291–319, 1984.
43. R. M. J. Cotterill J. C. Tallon Melting and the liquid glassy state, *J. Chem. Soc. Faraday Disc.*, **69**: 241–260, 1980.
44. H. P. Schwan R. J. Sheppard E. H. Grant Complex permittivity of water at 25°C, *J. Chem. Phys.*, **64**: 2257–2258, 1976.
45. V. V. Daniel *Dielectric Relaxation*, London: Academic Press, 1967, Chap. 7, pp. 95–109.
46. N. E. Hill W. E. Vaughan M. Davies *Dielectric Properties and Molecular Behaviour*, London: Van Nostrand Reinhold, 1969, Chaps. 3–5, pp. 191–461.
47. K. H. Illinger Dispersion and absorption of microwaves in gases and liquids, in J. B. Birks & J. Hart (eds.), *Progress in Dielectrics*, London: Academic Press, 1962, Vol. 4, pp. 37–101.
48. H. G. Sutter Dielectric polarization in gases, in M. Davies (ed.), *Dielectric and Related Molecular Processes*, London: Chemical Society, 1972, Vol. 1, Chap. 3, pp. 64–99.
49. E. H. Grant T. J. Buchanan H. F. Cook Dielectric behaviour of water at microwave frequencies, *J. Chem. Phys.*, **26**: 156–161, 1957.
50. J. B. Hasted Dielectric properties of water and of aqueous solutions, in M. Davies (ed.), *Dielectric and Related Molecular Processes*, London: Chemical Society, 1972, Vol. 1, Chap. 5, pp. 121–161.
51. R. J. Meakins Mechanism of dielectric absorption in solids, *Progr. Dielectr.* **3**: 151–202, 1961.
52. M. L. Williams R. F. Landel J. D. Ferry The temperature dependence of relaxation mechanisms in amorphous polymers and other glass-forming liquids, *J. Amer. Chem. Soc.*, **77**: 3701–3707, 1955.
53. D. K. Das-Gupta R. S. Brockley A study of absorption currents in polypropylene, *J. Phys. D Appl. Phys.*, **11**: 955–962, 1978.
54. C. Hall *Polymer Materials: An Introduction for Technologists and Scientists*, 2nd ed., London: Macmillan Education, 1989, Chap. 2, pp. 34–54.
55. R. T. Baily A. M. North R. A. Pethrick *Molecular Motions in High Polymers*, Oxford: Clarendon, 1981.
56. K. Deguchi E. Okaane E. Nakamura Effects of deuteration on the dielectric properties of ferroelectric CsH₂PO₄, 1. Static dielectric properties, *J. Phys. Soc. Japan*, **51**: 3569–3574, 1969.
57. P. R. Mason J. B. Hasted L. More The use of statistical theory in fitting equations to dielectric dispersion data, *Adv. Mol. Rel. Proc.*, **6**: 217–232, 1974.
58. M. Shablakh R. M. Hill L. A. Dissado Dielectric examination of glass-forming system, *J. Chem. Soc. Faraday Trans. 2*, **78**: 639–655, 1982.
59. M. Shablakh L. A. Dissado R. M. Hill Structure and dielectric relaxation mechanisms in the cyclic alcohols, cyclopentanols for cyclo-octanol, *J. Chem. Soc. Faraday Trans. 2*, **79**: 369–417, 1983.
60. L. A. Dissado R. M. Hill Dielectric behaviour of materials undergoing dipole alignment transitions, *Phil. Mag. B*, **41**: 625–642, 1980.
61. L. A. Dissado R. M. Hill Dynamic scaling and the first order character of ferroelectric transitions, *J. Phys. C*, **16**: 4023–4039, 1983.
62. P. C. Hohenberg B. I. Halperin Theory of dynamic critical phenomena, *Rev. Mod. Phys.*, **49**: 435–479, 1977.
63. L. A. Dissado R. M. Hill Examination of the dielectric susceptibility of poly-*r*-benzyl-L-glutamate, *J. Chem. Soc. Faraday Trans. 2*, **78**: 81–93, 1982.
64. L. A. Dissado J. C. Fothergill *Electrical Degradation and Breakdown in Polymers*, London: Peregrinus, 1992, pp. 74–116.
65. L. Reich S. A. Stivala *Elements of Polymer Degradation*, New York: McGraw-Hill, 1971, pp. 1–275.
66. T. Hibma H. R. Zeller Direct measurement of space charge injection from a needle electrode into dielectrics, *J. Appl. Phys.*, **59**: 1614–1620, 1986.
67. H. R. Zeller Thermodynamics of water treeing, *IEEE Trans. Electr. Insul.*, **EI-22**: 677–681, 1987.
68. R. Ross J. J. Smit Composition on growth of water trees in XLPE, *IEEE Trans. Electr. Insul.*, **27**: 519–530, 1992.

40 DIELECTRIC PERMITTIVITY AND LOSS

69. E. F. Steenis Water treeing in polymer cable insulations, *KEMA Sci. Tech. Rep. (ISSN 0167-8590)*, **8**: 149–208, 1990.
70. E. F. Steenis F. H. Kruger Water treeing in polyethylene cables, *IEEE Trans. Electr. Insul.*, **5**: 989–1028, 1990.
71. J. J. Xu S. A. Boggs The chemical nature of water treeing: theories and evidence, *IEEE Electr. Insul. Mag.*, **10**(5): 29–37, 1994.
72. H. J. Henkel et al. Relationship between the chemical structure and the effectiveness of additives in inhibiting water-trees, *IEEE Trans. Electr. Insul.* **EI-22**: 157–161, 1987.
73. A. Garton et al. Oxidation and water tree formation in service-aged XLPE cable insulation, *IEEE Trans. Electr. Insul.*, **22**: 405–412, 1987.
74. R. J. Densley et al. Water treeing and polymer oxidation, *conf. Record, Int. Symp. on Electrical Insulation*, IEEE Publ. 90-CH2727-6, 1990, pp. 178–182.
75. P. C. N. Scarpa A. Svatik D. K. Das-Gupta Dielectric spectroscopy of polyethylene in the frequency range of 10^{-5} Hz to 10^6 Hz, *Polym. Eng. Sci.*, **36**: 1072–1080, 1996.
76. M. Eigen G. Kurtze K. Tamm Zum Reaktionsmechanismus der Ultraschallabsorption in Wässrigen Electrolytlösungen, *Electrochemistry*, **57**: 103–118, 1957.
77. J. C. Chan S. M. Jaczek The moisture absorption of XLPE cable insulation under simulated service condition, *IEEE Trans. Electr. Insul.*, **EI-13**: 194–197, 1978.
78. H. Li The association of ions and electrical properties with water treeing in low density polyethylene, PhD Thesis, University of Strathclyde, UK, 1993.
79. D. K. Das-Gupta Conduction mechanisms and high field effects in synthetic insulating polymers, *IEEE Trans. Electr. Insul.*, **4**: 149–156, 1997.

D. K. DAS-GUPTA
University of Wales School of Electronic
Engineering and Computer Systems